

## INFORMATION TO USERS

This manuscript has been reproduced from the microfilm master. UMI films the text directly from the original or copy submitted. Thus, some thesis and dissertation copies are in typewriter face, while others may be from any type of computer printer.

**The quality of this reproduction is dependent upon the quality of the copy submitted.** Broken or indistinct print, colored or poor quality illustrations and photographs, print bleedthrough, substandard margins, and improper alignment can adversely affect reproduction.

In the unlikely event that the author did not send UMI a complete manuscript and there are missing pages, these will be noted. Also, if unauthorized copyright material had to be removed, a note will indicate the deletion.

Oversize materials (e.g., maps, drawings, charts) are reproduced by sectioning the original, beginning at the upper left-hand corner and continuing from left to right in equal sections with small overlaps. Each original is also photographed in one exposure and is included in reduced form at the back of the book.

Photographs included in the original manuscript have been reproduced xerographically in this copy. Higher quality 6" x 9" black and white photographic prints are available for any photographs or illustrations appearing in this copy for an additional charge. Contact UMI directly to order.



University Microfilms International  
A Bell & Howell Information Company  
300 North Zeeb Road, Ann Arbor, MI 48106-1346 USA  
313 761-4700 800 521-0600



**Order Number 1345284**

**Charge division in a cylindrical drift chamber for E1097**

**Gaussiran, Thomas Louis, II, M.A.**

**Rice University, 1991**

**U·M·I**  
300 N. Zeeb Rd.  
Ann Arbor, MI 48106



RICE UNIVERSITY

**CHARGE DIVISION IN A CYLINDRICAL DRIFT CHAMBER  
FOR E1097**

by

THOMAS L. GAUSSIRAN II

A THESIS SUBMITTED  
IN PARTIAL FULFILLMENT OF THE  
REQUIREMENTS FOR THE DEGREE  
MASTER OF ARTS

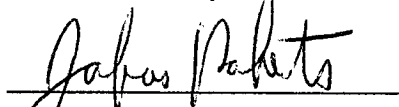
APPROVED, THESIS COMMITTEE



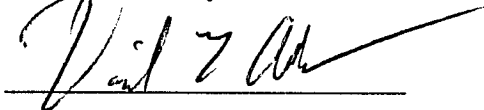
Billy E. Bonner, Chairman  
Chairman, Department of Physics  
Director, T.W. Bonner Nuclear Laboratory  
Professor of Physics



Gordon S. Mutchler  
Professor of Physics



Jabus B. Roberts  
Professor of Physics



David L. Adams  
Faculty Fellow

Houston, Texas

March, 1991

## **ABSTRACT**

### **CHARGE DIVISION IN A CYLINDRICAL DRIFT CHAMBER FOR E1097**

by

**THOMAS L. GAUSSIRAN II**

A review of the key concepts in the operation of a drift chamber are given. The equations governing charge division are developed. In order to optimize the chamber geometry, calculations were performed so that a suitable geometry for the chamber could be chosen. Electronics to determine position information along the wire (charge division) from the pulses at the two ends of the wire were designed and constructed. A test chamber was constructed and used to demonstrate the validity of the calculations as well as the ability of the electronics to make the position measurement. Results from tests using cosmic rays demonstrate position resolution to have a  $\sigma$  of less than 4 mm.

## ACKNOWLEDGEMENTS

I would like to thank my parents and family for helping me finish this thesis. They offered not only moral support but also took care of me when I was too busy to take care of myself. It would have almost impossible without their help. I hope my mom sees that she does understand physics. And I hope that I didn't babble too much. Thanks also to my advisors Billy Bonner and David Adams. Thanks especially to David for the many things he has taught me about experimental physics. Thanks to Alan Mattingly for listening to my troubles and helping me understand the physics behind the project. Thanks to Kathleen Johnston for getting the final data sets as well as helping me with the chamber. Also, thanks to John Clement for helping me bring up the PDP on Christmas Eve. And thanks to James Buchanan for his electronics expertise and help. Finally, I would like to thank Jin for her patient endurance, understanding and love.

# CHARGE DIVISION IN A CYLINDRICAL DRIFT CHAMBER FOR E1097

|   |           |
|---|-----------|
| <b>Chapter 1: Introduction.....</b>                             | <b>1</b>  |
| 1.1. Overview of E1097.....                                     | 1         |
| 1.2. Requirements on Chamber.....                               | 3         |
| 1.3. Overview of the paper.....                                 | 3         |
| <b>Chapter 2: Key Concepts.....</b>                             | <b>4</b>  |
| 2.1. Review of Wire Chambers.....                               | 4         |
| 2.1.1. Energy Loss In Matter .....                              | 4         |
| 2.1.2. Gases Used in Drift Chambers .....                       | 5         |
| 2.1.3. Multiplication .....                                     | 6         |
| 2.1.4. Choice of a Drift Chamber .....                          | 7         |
| 2.2. Drift Time.....  | 8         |
| 2.3. Charge Division.....                                       | 10        |
| 2.3.1. Introduction .....                                       | 10        |
| 2.3.2. Derivation .....   | 10        |
| 2.4. Gas mixture.....   | 13        |
| 2.4.1. Effects of Gases.....                                    | 13        |
| <b>Chapter 3: MWDC- A Drift Chamber Simulation Program.....</b> | <b>15</b> |
| 3.1. Introduction.....  | 15        |
| 3.2. Input Files .....  | 15        |
| 3.3. Output .....   | 17        |
| 3.4. Calculate Potential .....                                  | 18        |
| 3.5. Ionizing particle .....                                    | 20        |
| 3.6. Drift Electrons.....                                       | 20        |
| 3.7. Improvements.....  | 21        |
| 3.8. Wire Geometry.....   | 21        |
| <b>Chapter 4: Electronics.....</b>                              | <b>23</b> |
| 4.1. Introduction.....  | 23        |
| 4.2. Preamps and Preamp Boards.....                             | 24        |
| 4.2.1. Position Measurement Errors Due to Preamps.....          | 24        |
| 4.2.2. Design of Preamp Board .....                             | 29        |
| 4.2.3. Requirements .....                                       | 29        |



|                    |  |           |
|--------------------|--|-----------|
| 4.3.               | Receiving Board .....                        | 31        |
| 4.3.1.             | Introduction .....                           | 31        |
| 4.3.2.             | Design .....                                 | 31        |
| 4.3.3.             | Component Choices.....                       | 32        |
| 4.4.               | Digitizers.....                              | 33        |
| <b>Chapter 5:</b>  | <b>Results.....</b>                          | <b>35</b> |
| 5.1.               | Introduction.....                            | 35        |
| 5.2.               | Design.....                                  | 35        |
| 5.3.               | Single Wire Measurements .....               | 36        |
| 5.4.               | Test Chamber Measurements.....               | 38        |
| <b>Chapter 6:</b>  | <b>Conclusions.....</b>                      | <b>44</b> |
|                    | Improvements and Extensions .....            | 44        |
| <b>Appendix A:</b> | <b>MWDC a users guide .....</b>              | <b>45</b> |
| <b>Appendix B:</b> | <b>Jacobi Elliptic Functions.....</b>        | <b>48</b> |
| <b>Appendix C:</b> | <b>Cylindrical Chamber Construction.....</b> | <b>53</b> |

## List of Figures

|  |    |
|--|----|
| Fig. 1.1 E1097 Experimental Detector.....  | 2  |
| Fig 2.1 Plot of energy loss in Argon gas at STP vs energy of ionizing proton. ....                 | 5  |
| Fig 2.2 Terminal drift velocity for electrons vs applied electric field.....                       | 9  |
| Fig 2.3 Schematic of charge division.....  | 10 |
| Fig 2.4 Plot of the error in position measurement along the wire. ....                             | 12 |
| Fig 3.1 Layer of cylindrical chamber calculated by MWDC seen in cross section. ....                | 17 |
| Fig 3.2 Geometry used to compute potential using the solution obtained by Morse and Feshbach. .... | 19 |
| Fig 4.1 Schematic of the electronics used for E1097. ....  | 23 |
| Fig 4.2 Effects in position calculation caused by unequal gains in preamps. ....                   | 25 |
| Fig 4.3 Saturation of LeCroy preamp as a function of input charge. ....                            | 26 |
| Fig 4.4 Effects of non-linearity of preamps on position calculation.....                           | 27 |
| Fig 4.5 Error in position measurement due to incorrect input impedance ....                        | 28 |
| Fig. 4.6 Position error due to variation of the input impedance ....                               | 28 |
| Fig 4.7 Front of the preamp board. ....  | 30 |
| Fig 4.8 Back of the preamp board.....  | 30 |
| Fig 5.1 Present test chamber hole pattern found in the endcaps. ....                               | 36 |
| Fig 5.2 Position Resolution.....   | 37 |
| Fig 5.3 Position Calculation ....  | 38 |
| Fig 5.4 Side view and end view of test chamber.....  | 39 |
| Fig 5.5 Typical FERA spectra from a single wire in the test chamber.....                           | 40 |
| Fig 5.6 Histogram of multiplicity ....   | 41 |
| Fig 5.7 Residuals.....   | 42 |
| Fig B.1 Geometry used to compute potential ....  | 48 |
| Fig C.2 Cylindrical chamber design.....  | 53 |
| Fig C.2 Endcap for cylindrical drift chamber ....  | 54 |
| Fig C.3 Plastic feedthru, copper tube and wire.....  | 54 |
| Fig C 4 Layers of cylinder in cross section ....   | 57 |

# **CHARGE DIVISION IN A CYLINDRICAL DRIFT CHAMBER**

## **FOR E1097**

### **Chapter 1: Introduction**

#### **1.1. Overview of E1097**

Los Alamos E1097 [1][2] is an experiment to look at the reaction  $pn \Rightarrow pp\pi^-$ . The reaction  $NN \Rightarrow NN\pi$  is one of the simplest inelastic processes to study. From studying this reaction we can gain an understanding of NN and  $N\pi$  interactions, as well as understanding pion production. There are 3 channels available for this process. They can be expressed in terms of the total isospin of the nucleons for the initial (I) and final states (I'). The main channel in this reaction is  $(I, I') = (1, 0)$  which can proceed through the production of an intermediate  $\Delta^{++}$ . The reaction  $pn \Rightarrow pp\pi^-$  may proceed only through the (1,1) and (0,1) channels. This means that we will be able to study the non-resonant contributions to this process. The experiment is aided by the fact that all the final state particles are charged, allowing effective tracking.

Experiment 1097 will measure the differential cross section and the spin observables  $A_{N0}$ ,  $A_{L0}$ ,  $A_{S0}$ ,  $A_{0L}$ ,  $A_{SL}$ ,  $A_{NL}$ , and  $A_{LL}$  for the reaction  $pn \Rightarrow pp\pi^-$  for neutron beam energies 500-800 MeV. The first subscript for the spin observables refers to the polarization of the beam and covers the full range S, N, L, and 0 where 0 is unpolarized. The directions S, N, L form a right-handed coordinate system with N perpendicular to the scattering plane and L along the beam direction. The second subscript refers to the polarization of the target. The cross section with polarized beam and an L-type target can be expressed in terms of the unpolarized cross section  $\sigma_0$ , the beam polarization ( $p_S, p_N, p_L$ ), the target polarization (0,0, $p_T$ )

$$\sigma = \sigma_0 [1 + A_{S0} P_S + A_{N0} P_N + A_{L0} P_L + A_{SL} P_S P_T + A_{NL} P_N P_T + A_{LL} P_L P_T] \quad \text{Eq 1.1}$$

The floor plan of the experiment is shown in Fig 1.1. The neutron beam enters from the lower left side of the figure. The drift chamber is surrounded by scintillator bars which will be used as a first level trigger as well as for timing. The target is at the center of the chamber. The experiment is to be run in three phases. Phase 0 and 1 will use unpolarized targets and in Phase 2 a polarized target will be used.

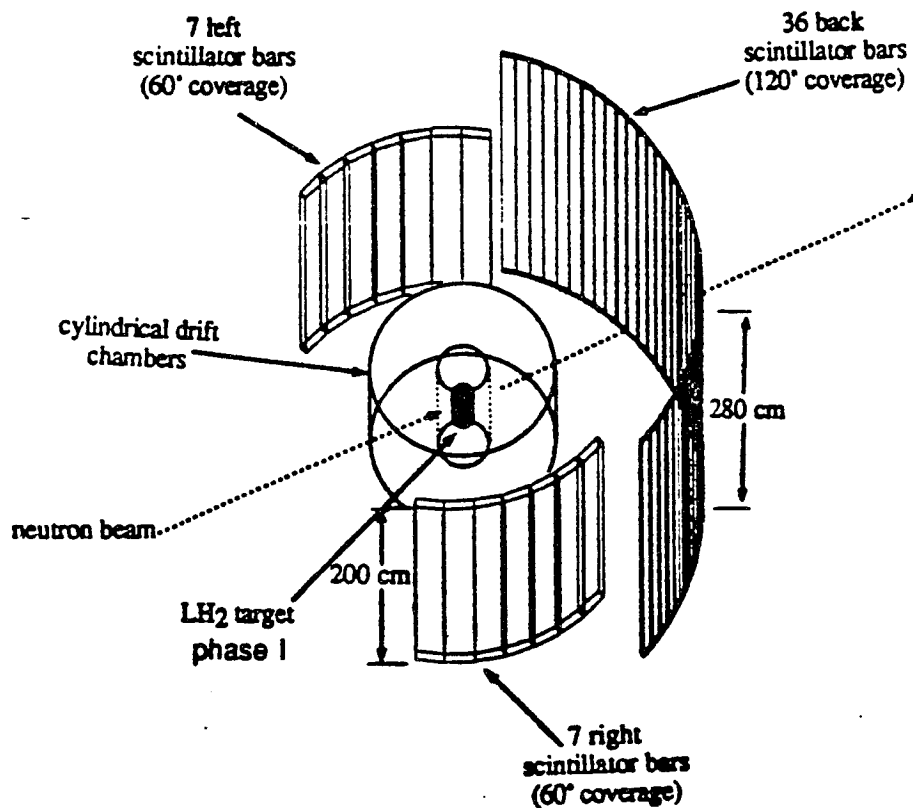


Fig. 1.1 E1097 Experimental Detector

## **1.2. Requirements on Chamber**

The heart of the experiment is a cylindrical drift chamber with an anticipated resolution of better than a mm in the drift direction ( $r\phi$ ). The position along the wire ( $z$ ) is measured using charge division and we have a goal of a resolution of a few mm. The latter measurement is the main subject of this dissertation. Note that the chamber is oriented with its axis vertical and the beams enters horizontally. The chamber has a large acceptance:  $\pm 60^\circ$  vertical angular acceptance and  $\pm 120^\circ$  horizontal acceptance. This gives the chamber full acceptance for the protons and will accept 75% of the pions produced.

## **1.3. Overview of the paper**

This thesis reports on several tasks undertaken in preparation for the experiment.

1. In order to optimize the chamber geometry, calculations were performed so that a suitable geometry for the chamber could be chosen.
2. Electronics to determine position information along the wire from the pulses at the two ends of the wire were designed and constructed.
3. A test chamber was constructed and used to demonstrate the validity of the calculations as well as the ability of the electronics to make the position measurement.
4. Results from tests using cosmic rays will be presented.

## Chapter 2: Key Concepts

### 2.1. Review of Wire Chambers

In this section we will review the main concepts in the use of a multi-wire drift chamber utilizing charge division. In a wire chamber a charged particle passes through the gas of the chamber and ionizes gas atoms along the track. The electrons produced from this ionization drift towards a sense wire. Near the sense wire multiplication occurs which allows detection of the signal.

#### **2.1.1. Energy Loss In Matter**

The amount of energy deposited per unit length is given by the Bethe-Bloch equation: [3]

$$\frac{dE}{dx} = -K \frac{Z}{A} \frac{\rho}{\beta^2} \left\{ \ln \frac{2mc^2\beta^2 E_M}{I^2(1-\beta^2)} - 2\beta^2 \right\}, \quad K = \frac{2\pi N z^2 e^4}{mc^2} \quad \text{Eq 2.1}$$

Where N is Avogadro's number, m and e are the electron mass and charge, Z, A and  $\rho$  are the atomic number and mass and the density of the medium, I is its effective ionization potential, z is the charge and  $\beta$  the velocity of the projectile. The parameter  $E_M$  is the maximum energy transfer allowed in each interaction. From two-body kinematics we obtain:

$$E_M = \frac{2mc^2\beta^2}{1-\beta^2}. \quad \text{Eq 2.2}$$

Fig 2.1 shows  $dE/dx$  for Argon at STP as a function of the incident proton energy. Note the minimum ionizing particle has an energy of about 1 GeV. On the same plot one may read the number of electrons produced by the ionizing particle per cm.

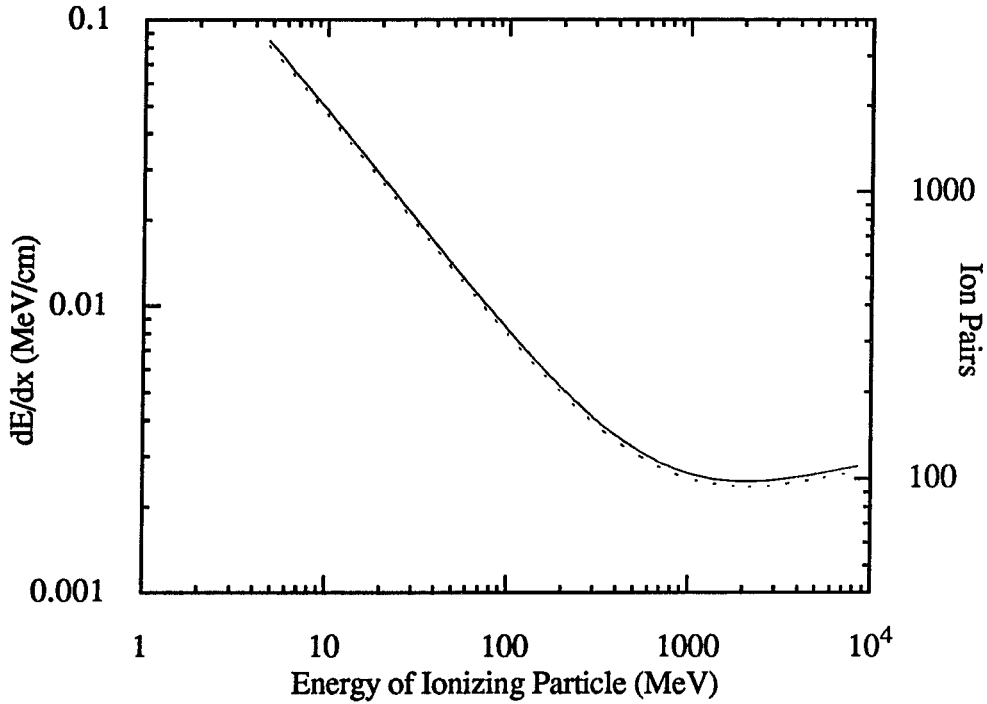


Fig 2.1 Plot of energy loss in Argon gas at STP vs energy of ionizing proton. The right axis shows the number of ion pairs produced in the Argon

### 2.1.2. Gases Used in Drift Chambers

The various parameter for many of the gases commonly used in drift chamber have been measured empirically. A tabulation of these data has been given by Sauli.[4] In table 2.1 we reproduce some of this information. Here  $Z$  and  $A$  are the atomic number,  $\rho$  is the density,  $I_0$  allows the calculation of the effective ionization potential  $I$  using the simple formula  $I = I_0 Z$ . Also  $W_i$  is the amount of energy that is deposited in order to produce an ion pair (ip). The quantity  $dE/dx$  is the amount of energy lost per unit length by a minimum ionizing particle in both reduced units and normal. Finally, we have the values of  $n_p$  and  $n_t$  which are the number of primary and total ion pairs produced by an minimum ionizing

particle per cm. Note that  $n_t$  and  $W_i$  are related by  $n_t = \frac{\Delta E}{W_i}$  where  $\Delta E$  is the total energy lost in a gas volume.

| Gas                            | Z  | A    | $\rho$<br>(g/cm <sup>3</sup> ) | $I_0$<br>(eV) | $W_i$<br>(eV) | $\frac{dE}{dx}$<br>(MeV/gcm <sup>-2</sup> ) | $\frac{dE}{dx}$<br>(keV/cm) | $n_p$<br>(ip/cm) | $n_t$<br>(ip/cm) |
|--------------------------------|----|------|--------------------------------|---------------|---------------|---|-----------------------------|------------------|------------------|
| Ar                             | 18 | 39.9 | $1.66 \times 10^{-3}$          | 15.8          | 26            | 1.47  | 2.44                        | 29.4             | 94               |
| C <sub>4</sub> H <sub>10</sub> | 34 | 58   | $2.42 \times 10^{-3}$          | 10.8          | 23            | 1.86  | 4.50                        | (46)             | 195              |

Table 2.1 Characteristics of two main gas constituents to be used in the cylindrical chamber for E1097.

### 2.1.3. Multiplication

The fate of the electrons which are produced from the ionizing particle depends on the applied voltage. At low voltages the electrons are lost to recombination with the ions. As the voltage is turned up, the electric field near the wire becomes large enough to start multiplication.

Once the threshold for multiplication has been crossed, the electron traveling towards the sense wire scatters from atoms freeing other electrons. The electric field increases as  $1/r$  finally becoming large enough to accelerate the electron above the ionization threshold. These electrons free others and there is a cascade of negative charge towards the sense wires as the ions head towards the high voltage wires. The multiplication can become quite large ( $10^8$  or larger). In fact the amount of the multiplication,  $M$ , from the primary electrons goes up exponentially with the high voltage: [4]

$$\log M = \int_{x_i}^{x_f} \alpha(x) dx$$



Where  $\alpha(x)$  is the first Townsend coefficient and represents the number of ion pairs produced per unit length of drift, it is defined as follows:

$$\alpha(x) = A p \exp \left\{ \frac{-B p}{E(x)} \right\}$$

$$\text{where } A = 14 \text{ Torr}^{-1} \text{ cm}^{-1} \text{ and } B = 180 \text{ V Torr}^{-1} \text{ cm}^{-1} \quad \text{Eq 2.3}$$

If the voltage is turned up further the chamber eventually enters a Geiger-Muller mode in which the length of the wire is surrounded by electrons. After this it enters a regime of continuous discharge.

#### 2.1.4. Choice of a Drift Chamber

In a proportional chamber position information is gained by having closely spaced wires and recording the address of each hit wire. Therefore, the position resolution is determined by the spacing of the wires. A drift chamber uses wires with coarser spacing than a proportional chamber but by measuring the drift time one can obtain position resolution at the 100 micron level. The benefits of a drift chamber over a proportional chamber are that fewer channels are needed and better resolution is achieved. The drawback is that the electronics for each channel are more complicated requiring a TDC for each wire.

Both of these methods only give two dimensional coordinates. That is due to the fact that the position along the length of the wire is not known. One technique for determining the other coordinate is to use multiple planes with different orientations. If multiple tracks are present, usually three or more orientations are used to resolve ambiguities. This method significantly increases the channel count and the complexity of the track reconstruction algorithm. There are also some geometrical difficulties in applying this method to cylindrical chambers.

For these reasons, we use charge division to determine the third coordinate. The position of the track in the plane perpendicular to the wire is measured by the drift time as

in a standard drift chamber. The position along the wire is measured by charge division, which makes use of the ratio of the charges collected at each end of the wire. This means that only one layer of wires is needed in order to obtain a three dimensional coordinate. The drawback to this method is that two ADC channels and one TDC channel are needed for each wire. Also, the precision of the measurement of the position along the wire is typically 1% of the wire length.

## **2.2. Drift Time**

The drift time is measured with respect to a fast trigger. This can be done by using a pair of scintillators one in front and one behind the chamber. The coincidence between the two scintillators generates the start for a TDC. The stop pulse comes from the chamber when the electrons from the ionizing particle cascade onto the sense wire. Due to collisions with the gas, the electrons and the ions quickly reach a terminal velocity. This final velocity depends on the gas mixture: for a 70-30 Argon/Isobutane mixture, it is about 50 mm/ $\mu$ s for the electron. In an experiment of this type the drift distances will be correlated to a drift time by calibration. The drift velocity has been tabulated by Sauli [4] as a function of the electric field in different Argon/Isobutane mixtures. This data is shown in Figure 2.2. Note that the drift speed is insensitive to the exact gas mixture and field over the chamber's working range.

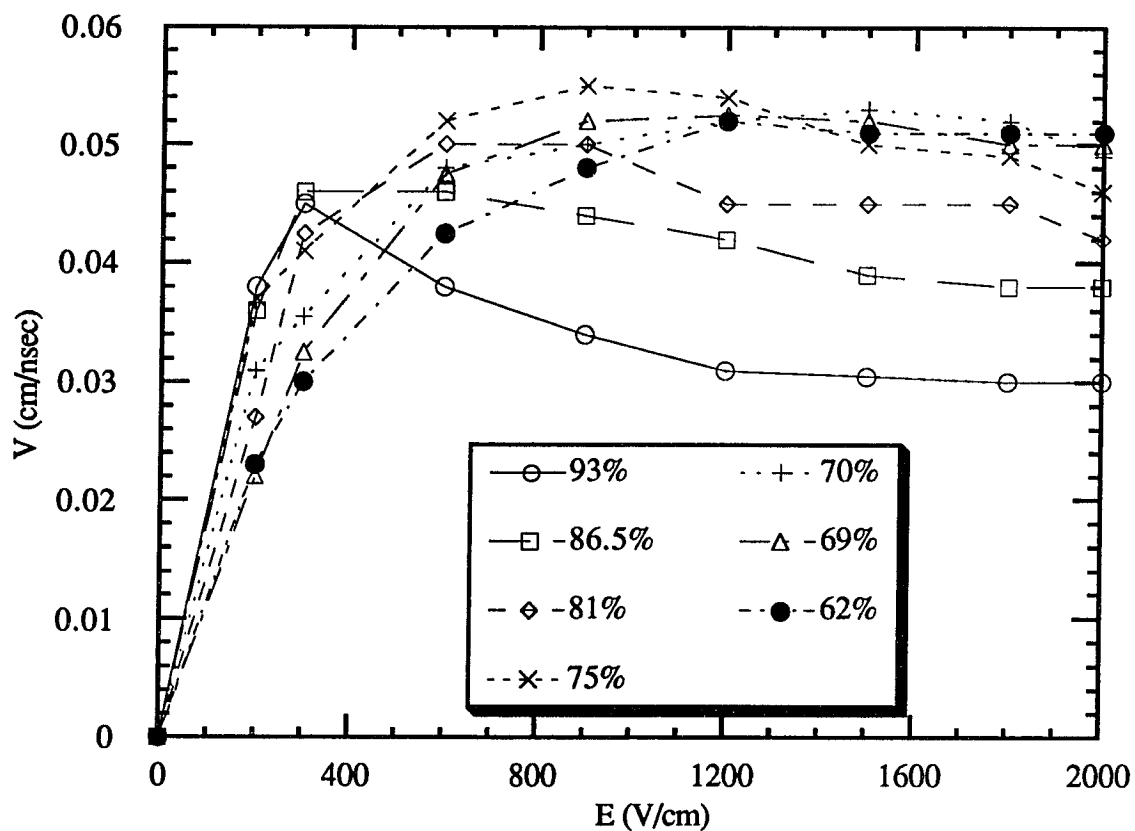


Fig 2.2 Terminal drift velocity for electrons vs applied electric field. The various curves show the change due to percentage of Argon in an Argon / Isobutane mixture.

A difficulty inherent to wire chambers is that it is ambiguous as to which side of the wire the particle passed. Each of the four measuring layers in the cylindrical chamber consists of two planes of wires offset by half a wire spacing. This allows the resolution of this left-right ambiguity.

## 2.3. Charge Division

### 2.3.1. Introduction

The position along the wire is computed using a technique known as charge division. This method uses a technique familiar from elementary electronics known as a divider circuit. See Fig 2.3.

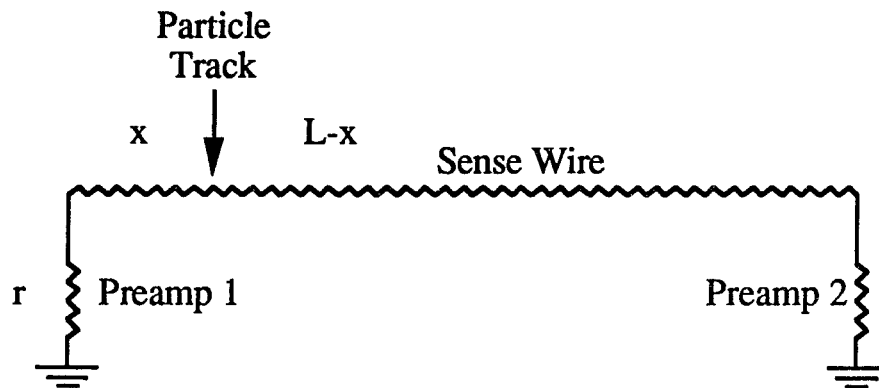


Fig 2.3 Schematic of charge division. The preamps on either end of the wire have an input resistance  $r$ . While the sense wire has an overall resistance of  $R$ .

### 2.3.2. Derivation

It can be shown that for a wire with total resistance  $R$ , output resistance of  $r$  (due to the input impedance of the preamps), and at a position  $x$  along a wire of length  $L$ ; that the charge on each end can be written as follows:

$$Q_1 = \frac{\rho + \frac{x}{L}}{1 + 2\rho} \quad Q_2 = \frac{\rho + (1 - \frac{x}{L})}{1 + 2\rho} \quad \text{Eq 2.4}$$

Where we have defined  $\rho = \frac{r}{R}$ . Define  $\gamma$  to be the ratio of the charges:

$$\gamma = \frac{Q_1}{Q_2} = \frac{\rho + \frac{x}{L}}{1 + \rho - \frac{x}{L}} \quad \text{Eq 2.5}$$

Then we can write the position along the wire as:

$$x = \frac{\gamma (1 + \rho) - \rho}{1 + \gamma} L \quad \text{Eq 2.6}$$

We now examine the question of precision in charge division and the conditions that must be satisfied for a desired precision. One can determine the variance in  $x$  with respect to  $\gamma$  by differentiation:

$$\Delta x = \frac{2\rho + 1}{(1 + \gamma)^2} \Delta \gamma L. \quad \text{Eq 2.7}$$

But we can write  $\Delta \gamma$  as

$$\Delta \gamma = \sqrt{1 + \gamma^2} (1 + \gamma) \frac{\Delta Q}{Q} \quad \text{Eq 2.8}$$

where we have set  $Q = Q_1 + Q_2$  and  $\Delta Q$  is to be the uncertainty in each charge measurement. Substituting this back and obtaining the expression for  $\Delta x$ :

$$\Delta x = (2\rho + 1) \frac{\sqrt{1 + \gamma^2}}{1 + \gamma} \frac{\Delta Q}{Q} L \quad \text{Eq 2.9}$$

Or in terms of the position on the wire:

$$\Delta x = \sqrt{(1 + 2\rho + 2\rho^2) - 2 \left(\frac{x}{L}\right) + 2 \left(\frac{x^2}{L^2}\right)} \frac{\Delta Q}{Q} L \quad \text{Eq 2.10}$$

Note that the error in  $\Delta x$  is proportional to the fractional error in the charge measurements  $\frac{\Delta Q}{Q}$ .

Or in the approximation that  $\rho \rightarrow 0$  this becomes simply:

$$\Delta x = \sqrt{1 - 2 \frac{x}{L} + 2 \frac{x^2}{L^2}} \frac{\Delta Q}{Q} L \quad \text{Eq 2.11}$$

In the cylindrical chamber  $\rho = 60 \, \Omega / 1716 \, \Omega = 0.035$  figure 2.4 shows how the ratio  $\frac{\Delta x / L}{\Delta Q / Q}$  varies as a function of  $x / L$  for this value of  $\rho$ .

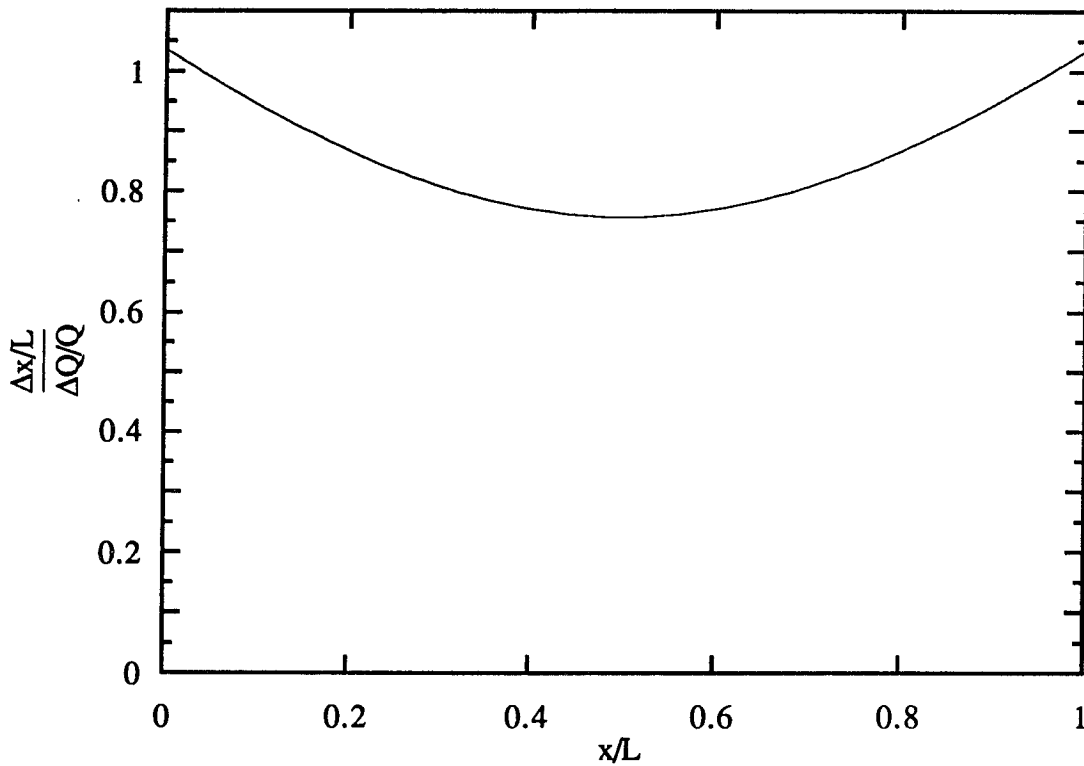


Fig 2.4 Plot of the error in position measurement along the wire.

Therefore, it is clear that the least amount of error is near the center of the chamber and that the precision improves linearly with the total charge and is inversely proportional to the error in the charge measurement. It is also interesting to note that the error does not depend strongly on the resistances.

## **2.4. Gas mixture**

The choice of gas is very important to the characteristics of how the chamber responds. The gas mixture has two main components: Argon and Isobutane. It may also contain other gases to fine tune the response.

### **2.4.1. Effects of Gases**

#### **Argon**

A noble gas is usually the main gas component in a wire chamber. This is due to the fact that noble gases can only be excited through photon emission or absorption, therefore avalanche multiplication occurs at much lower fields. Although Xenon and Krypton would give better multiplication they are not used due to the high cost. With pure Argon it is only possible to get multiplication on the order of  $10^3$ - $10^4$  before going into constant discharge. It is necessary to add additional gases to increase the multiplication.

#### **Isobutane**

The polyatomic atoms behave in a very different way from the noble gases. Polyatomic molecules with more than four atoms have a large number of non-radiative excited states. This means that they absorb photons over a wide energy range. Isobutane ( $C_4H_{10}$ ) has a very efficient absorption range which covers the range emitted by Argon. This prevention of secondary emissions permits gains up to  $10^6$ .

We can further modify the characteristics of the chamber by adding other gases. The most important of these for E1097 will be freon and methylal.

#### **Freon**

The main effect of freon is to absorb electrons. Although this may seem undesirable; it actually has the useful effect of absorbing stray electrons. Ionizing particles should free several electrons so these signals are able to make it to the sense wires. Since the number of

stray electrons is smaller, the voltage may be turned up which increases the gain, effectively increasing the signal to noise ratio. Therefore it is possible to get gains of around  $10^7$  before breakdown [4]. These very high gains correspond to a saturated signal, reducing the dynamic range. This may be important in matching to the dynamic range of the electronics.

Efficiency can be defined as the number of events above the pedestal divided by the total number of events. In testing this it was found that with 0.1% Freon added to the gas mixture, efficiency was only about 40%. Whereas with only Argon and Isobutane the efficiency was above 90%. Apparently the Freon was absorbing the drift electrons before they could begin to multiply.

#### Methylal

Another gas that we may add is methylal  $(\text{OCH}_3)_2\text{CH}_2$ , by bubbling Argon through methylal which has been chilled to  $0^\circ\text{C}$ . The addition of alcohols have been found to reduce ageing effects seen in some chambers. The methylal may also prevent "whiskers" on HV wires which have been noticed in other chambers. Although these whiskers are not completely understood, many believe that they arise from the ions that collect and polymerize on the HV wires. The effect of these whiskers is to shield the charge, which affects the field characteristics, and slows the recovery time of the chamber. It is also possible to build up enough of these whiskers so that they bridge to a sense wire and short that connection.



## **Chapter 3: MWDC- A Drift Chamber Simulation Program**

### **3.1. Introduction**

The program MWDC was written to simulate different geometries for drift cells, calculate multiplication on sense wires, track particles through a chamber, and track electrons produced by the ionizing particle. The program was based on a program written at University of Houston called DPLANE7. Many refinements have gone into the program from the original and little of it still remains. The program DPLANE7 was written to handle only a single geometry. MWDC uses a geometry which is defined in an input file and is much more flexible. Many of the other programs in the current literature assume an unnecessarily simple geometry and base the calculations on this model. [6-9]

### **3.2. Input Files**

The input file for MWDC contains three sets of information. First, it defines the geometry of the chamber. The program assumes that the chamber has a pair of parallel foils held at ground. The foils extend to infinity. Between these foils can be placed many sets of wires. Each of these sets consists of an infinite array of wires, all at the same distance from the foils and placed an equal distance apart. The most convenient way to describe this geometry is to define a unit cell which contains one wire from each of these sets. The position, voltage, and radius of this wire make up the input. Other information includes the plate separation and cell size. The next set consists of information describing the ionizing particle. This consists of including the type of particle, momentum and direction. The final set of information includes various parameters which can be changed such as gas mixture, pressure, and control parameters. A more complete description of an input file can be found in appendix A.

With the applied voltage and the geometry it is possible to calculate the charge on each wire. This process can be understood most easily in vector notation. Let us define a vector  $\vec{V}$  which is comprised of the voltages  $V_i$ , where  $V_i$  is the voltage applied to wire plane  $i$ , and a vector  $\vec{\lambda}$  which is the charge per unit length on each wire of each plane. The potential due to the charge on plane  $i$  can be written as  $V_i(x) = A_i(x) \lambda_i$ . In a moment we will discuss the function  $A_i(x)$ . For now we note that it depends only on the geometry and does not depend on  $\vec{V}$  or  $\vec{\lambda}$ .

The potential at any point in space can be written as:

$$V(x) = \sum_i A_i(x) \lambda_i. \quad \text{Eq 3.1}$$

We can evaluate this at the position of one of wires in plane  $j$  as:

$$\begin{aligned} V_j &= \sum_i V_i(x_j) \\ &= \sum_i A_{ji} \lambda_i \end{aligned} \quad \text{Eq 3.2}$$

where  $A_{ji} = A_i(x_j)$

In terms of matrix notation we can write this as  $\vec{V} = \mathbf{A} \vec{\lambda}$  and we can invert  $\mathbf{A}$  to obtain the charges in terms of the fixed potentials:  $\vec{\lambda} = \mathbf{A}^{-1} \vec{V}$ . Having determined the charges we can use Eq 3.1 to find the potential at any point in space.

The electric field can be calculated by taking the gradient of the potential. The electric field then affects the drift electron trajectories. It is possible to include a description of a magnetic field which affects the ionizing particle as well as the drift electrons.

### 3.3. Output

The following is a figure showing the equipotential lines of one of the layers of the cylindrical chamber. Also one can see the track of a 30 MeV proton passing through as well as the trail of drift electrons it has produced. A close inspection of this may reveal that certain tracks for the drift electrons simply stop, these tracks have timed out.

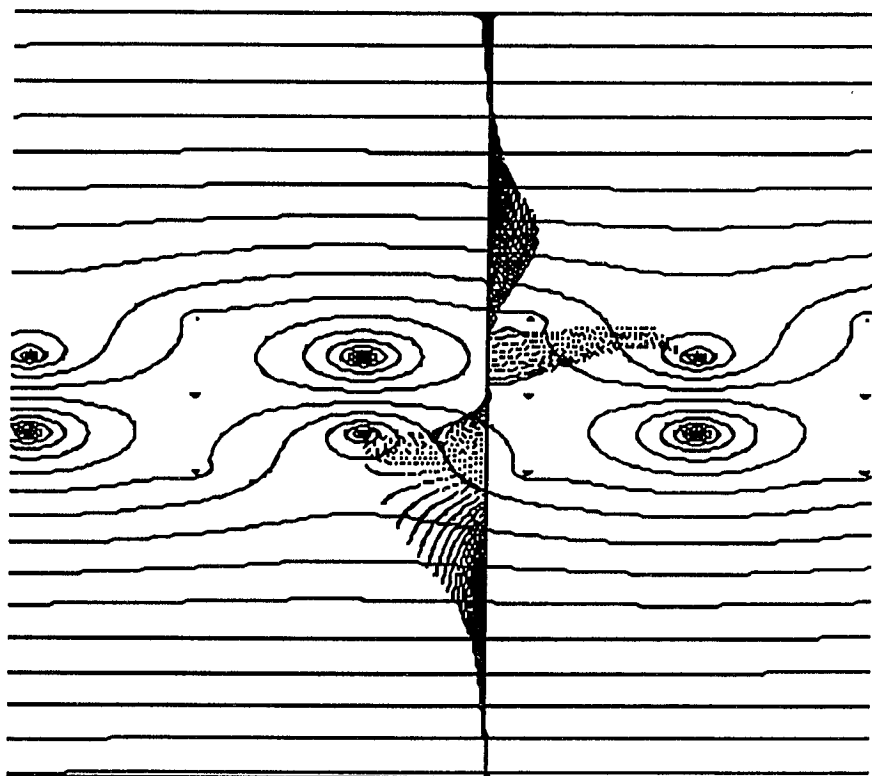


Fig 3.1 Layer of cylindrical chamber calculated by MWDC seen in cross section. The foils are found at the top and the bottom of the figure. Equipotential lines show the changing electric potential in 100 V steps. The wires are coming out of the page and are arranged in a hex pattern.

Confirmation of the accuracy of the program came during tests with the test chamber. We observed that with all the high voltage wires at the same potential, the center sense wires consistently had a larger signal than the wires close to the wall. This was at first

thought to be anomalous behavior in the chamber, but when it was checked against the MWDC prediction the code properly predicted the difference in multiplication that was seen. We were able to understand that this was due to the difference in geometry, and for all sense wires to have the same gain the high voltage wires will need different voltages. Now we can review in more detail the major tasks with which MWDC is concerned.

### **3.4. Calculate Potential**

The analytic solution to the wire chamber geometry requires the use of analytic functions known as the Jacobi elliptic functions. Using these functions and generalizing from a simpler problem, Morse and Feshbach obtain a closed form solution [10]. In order to find the potential at any point in space we need to evaluate this solution. Unfortunately, it is not convenient to compute the function in the form given by Morse and Feshbach since their solutions involve complex arguments for the functions. For a further discussion of some of the properties of these functions see appendix B or [11]. We will simply state the solution that satisfies the required boundary conditions.

Let us assume that we have one set of infinitely many wires arranged between two parallel plates. The wires are placed a distance  $2b$  apart and a distance  $x_0$  from one of the foils. The foils are placed a distance  $a$  apart. In the following figure the dark solid lines are the foils of the chamber viewed with the wires coming up out of the page. The wires are the  $+$  between the solid lines.

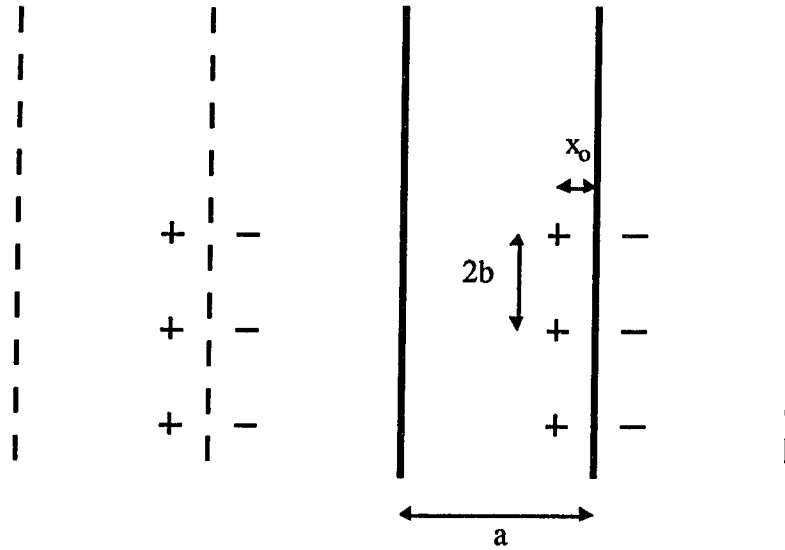


Fig 3.2 Geometry used to compute potential using the solution obtained by Morse and Feshbach.

The boundary conditions which must be met are that the function should be zero along the foils, there should be a positive going pole for each positive charge or positive image charge. And there should be a negative going pole for the negative image charges. If we set the right plane to be at  $x=0$  then the wires are located at  $z = x_0 + i 2nb$  for  $n=0, \pm 1, \pm 2, \dots$ . There are image charges of opposite sign at  $z = -x_0 + 2ma + i 2nb$  for  $m, n=0, \pm 1, \pm 2, \dots$  and image charges of the same sign for  $z = x_0 + 2ma + i 2nb$  for  $n= 0, \pm 1, \pm 2, \dots$  and  $m= \pm 1, \pm 2, \dots$ .

Leaving the details for later we state the solution of the potential at all points in space to be:

$$F(z) = -2q \operatorname{Re} \ln \left( \frac{\frac{\operatorname{cn}(2\theta)}{\operatorname{sn}(2\theta)} - \frac{\operatorname{cn}(\theta-\phi)}{\operatorname{sn}(\theta-\phi)}}{\frac{\operatorname{cn}(2\theta)}{\operatorname{sn}(2\theta)} - \frac{\operatorname{cn}(\theta)}{\operatorname{sn}(\theta)}} \right) \quad \text{Eq 3.3}$$

Where we have used the following definitions  $\theta = Kx_0/a$  and  $\phi = Kz/a$ . And  $K$  is the quarter period of the the Jacobi elliptic functions. The only part of this solution that changes with position has the form  $f(z) = \frac{\text{cn}(\theta - \phi)}{\text{sn}(\theta - \phi)}$ . This then is the piece we must investigate to check the boundary conditions. At  $z=0$ ,  $\phi=0$  and the argument of the logarithm is 1 and the first boundary condition is satisfied. The negative poles at  $z = -x_0 + 2ma + i 2nb$  for  $m, n=0, \pm 1, \pm 2, \dots$  are satisfied due to the periodicity of the Jacobi Elliptic Functions  $f = \frac{\text{cn}(2\theta)}{\text{sn}(2\theta)}$ . Therefore, the argument is zero. At the positions for positive poles we have that  $f$  has a positive pole because  $\text{sn}$  has a zero. The final boundary condition is along the foil at  $z=a$ . When this is evaluated the argument of the logarithm becomes -1 and so  $F(z)$  vanishes as required.

### **3.5. Ionizing particle**

Once the potential field is calculated over the cell an ionizing particle can be stepped through. The momentum and direction of the ionizing particle is described in the input file as well as the type of ionizing particle. As it steps through the chamber the particle sees the electric field generated by the wires as well as an externally imposed magnetic field. The magnetic field can either be described in functional form or by describing the field point by point as might be obtained from a zip-track scan.

### **3.6. Drift Electrons**

From the energy loss of the particle in the gas, electrons are produced. There is a characteristic number of electrons lost which is dependent on the particle and the gas mixture used.

These electrons are then released, their position stored, and their number calculated using the average number of electrons produced per cm times the step size. This number is then used as the average of a Poisson distribution; and a random number is chosen using this distribution. These electrons are now subject to the same fields as the ionizing particle and begin to drift towards the sense wires. The electrons soon achieve a maximum drift velocity which is limited by collisions with the gas molecules. This maximum velocity is again a function of the gas mixture used. The electrons are tracked until they reach a wire at which time the charge deposited, the wire hit, and the time of the impact is recorded.

### **3.7. Improvements**

There are a few improvements that might be useful to add to MWDC. First, the Morse and Feshbach solution is for a linear geometry; but it is possible to conformally map this solution to a cylindrical geometry. In this way we would have an exact calculation of the the electrostatic field and the multiplication of the cylindrical chamber. Second, it should be possible to include a  $\chi^2$  minimization routine with the ability to adjust the high voltage on the wires so that the same charge could be put on each of the sense wires. This would then ensure that all the sense wires have the same multiplication.

### **3.8. Wire Geometry**

Several different geometries were originally considered for the chamber. First, it was decided that the chamber should be a full right cylinder. This enables us to look at a great deal of the particles that might come from the reaction including back scattered particles. Not all of the chamber will be wired but that ability will exist if it is needed in the future. The local geometry will be a staggered hex pattern. The advantages to this arrangement of field shaping wires is that it minimizes the number of field wires. A possible problem with

this design is that dead areas exist, which may allow charge to build up, distort the field, and leak into adjacent cells giving false hits. Another problem with this geometry is that the cells in adjacent planes are not the same size. It was decided to keep the angular spacing in adjacent wire planes. This means that the inner cell of a layer is smaller than the outer one. This may cause variations in the gain of the wires, however these gain variations should be correctable by adjusting the high voltages properly.



## Chapter 4: Electronics

### 4.1. Introduction

As critical to this experiment as the chamber are the electronics for data collection. This can be broken into a three different parts: the preamp, discriminator, and digitizers. The electronics for the chamber are chosen to do a twofold job. First, the charge at each end of the wire must be measured very accurately (better than 1%). This gives us information about where the charged particle passed along the length of the wire. The second job is to measure the time from which the particle hits the scintillators till a signal on the chamber is seen. Since we can know the drift speed of electrons in the gas, we can then compute the distance the particle passed from the wire. By having several layers, it is then possible to resolve the left-right ambiguity. The figure 4.1 shows a schematic of the main divisions of the electronics. If delay cable is to be installed the ideal place would be between the preamp and the transformer.

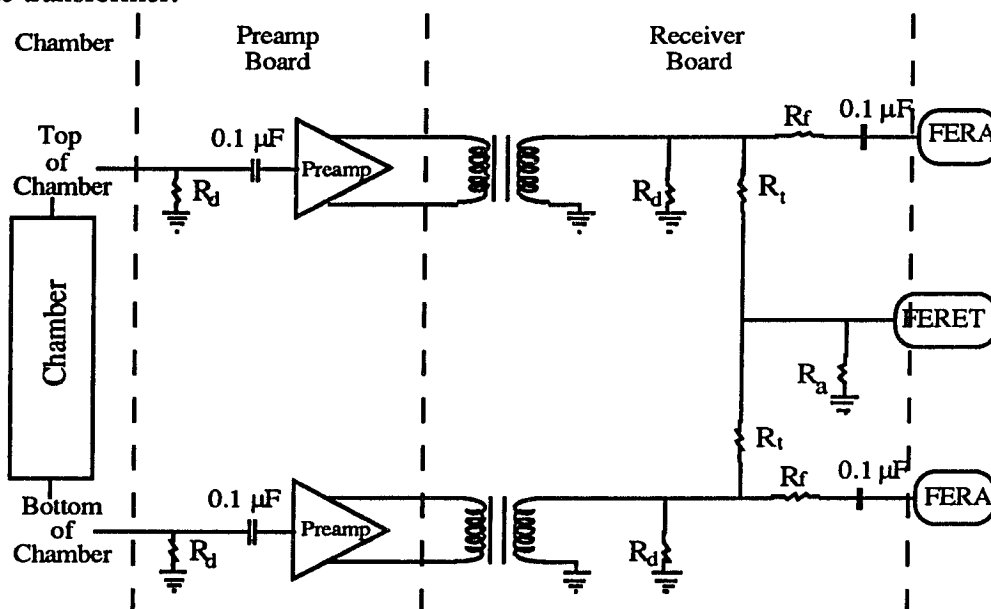


Fig 4.1 Schematic of the electronics used for E1097.

## **4.2. Preamps and Preamp Boards**

The signal from the sense wire is too small to drive the delay cable and then be digitized. The simple limitations of signal to noise and the inability (and undesirability) of using the chamber to drive the cable necessitates the use of preamps as close to the sense wires as possible. The preamp we have chosen to use is the LeCroy HQV101 model. It has a high charge gain  $\approx 48x$ , fast rise time  $\approx 20$  nsec, and a low input impedance  $\approx 60 \Omega$ . It can drive twisted pair cable which helps eliminate noise with common mode rejection.

Most of the work is done by the LeCroy preamp chip. A circuit board was designed and constructed to hold the preamps and supply them with power as well as conduct the signals in and out of the preamps. The signal comes from the chamber through a short shielded coaxial cable and onto the board. The signal then goes through a decoupling  $0.1 \mu\text{F}$  capacitor which is necessary because the preamp input is set at a level of about  $0.7 \text{ V}$ . The sense wire is also grounded through  $R_d = 10 \text{ k}\Omega$ . It bleeds off charge which builds up on the sense wires from the cascading  $e^-$ . Without it the signal soon disappears as the sense wire comes to the potential of the high voltage wires. Also, this resistor in conjunction with the  $0.1 \mu\text{F}$  capacitor it should protect the preamp as the high voltage is turned up or in case of a short.

### **4.2.1. Position Measurement Errors Due to Preamps**

In the calculations that follow it should be noted that the parameters used are those for the cylindrical chamber. These parameters are: total length of chamber 1 meter, resistance of sense wire per meter  $1560 \Omega$ , input impedance of the preamps  $60 \Omega$ . The following plot shows the effect on the gain if one of the preamps has a gain greater than the one on the opposite side of the wire by 1%, 5%, 10%, or 20%. It is clear that the position error is about 1% for a 5% gain increase.

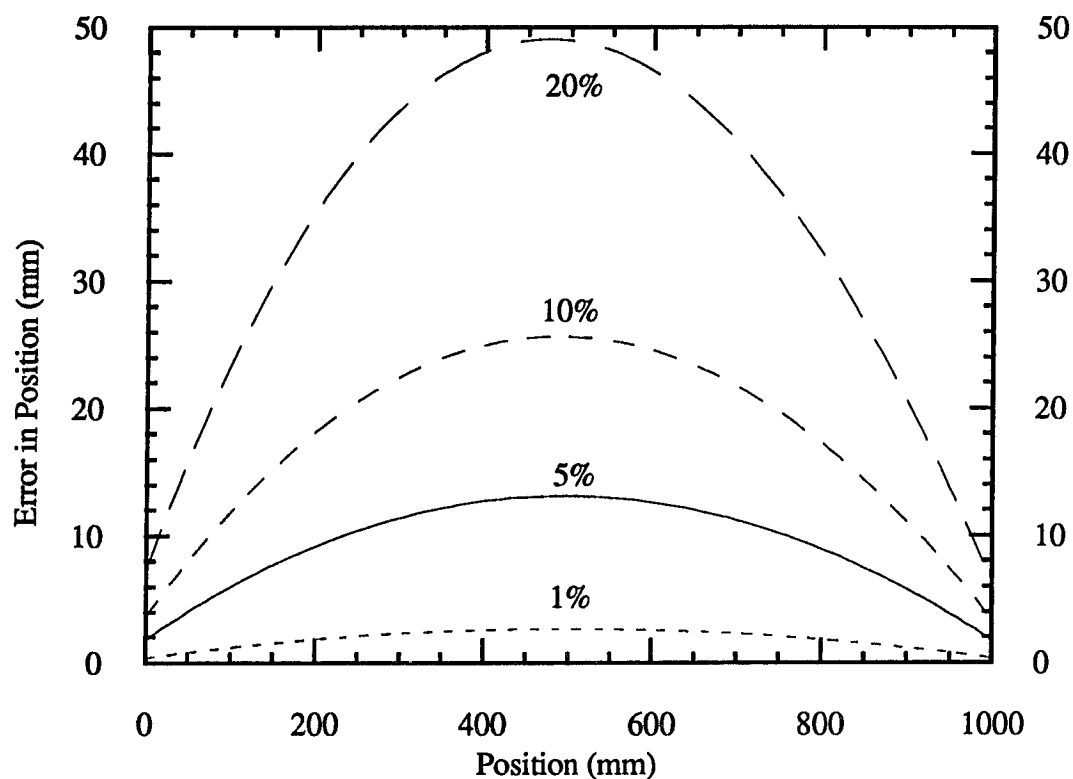


Fig 4.2 Effects in position calculation caused by unequal gains in preamps.

The figure 4.3 shows the results of a saturation test on a single preamp to see at what point it would become nonlinear. LeCroy states that they are non-linear for an input greater than 40 pC or  $2.5 \times 10^8 e^-$ . We found that although this is true the preamps are still stable and might be usable for inputs up to at least 400 pC.

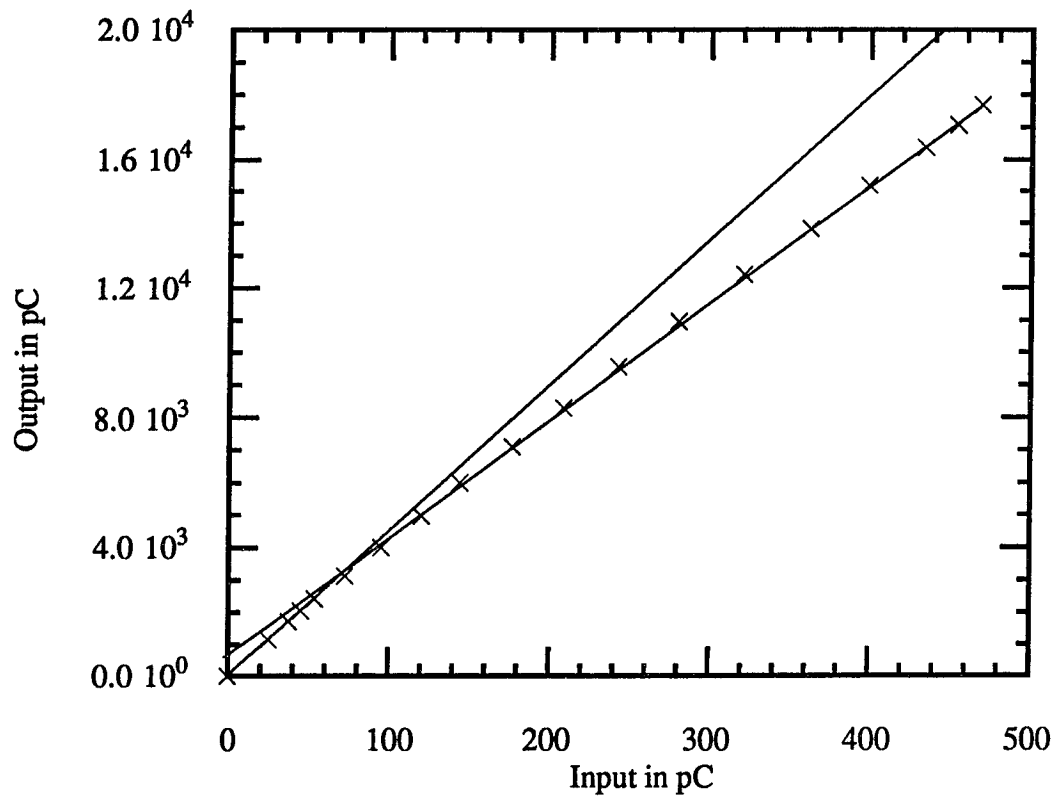


Fig 4.3 Saturation of LeCroy preamp as a function of input charge.

Next, we see the effects this saturation has on position calculation. The different curves in figure 4.4 represent different input charge to the preamps. One can see that as expected the error in position calculation becomes worse as the saturation effect becomes greater. It should be clear that if the chamber is driven at such a voltage as to produce currents above the linear point of the preamps that it will be necessary to correct the position calculation.

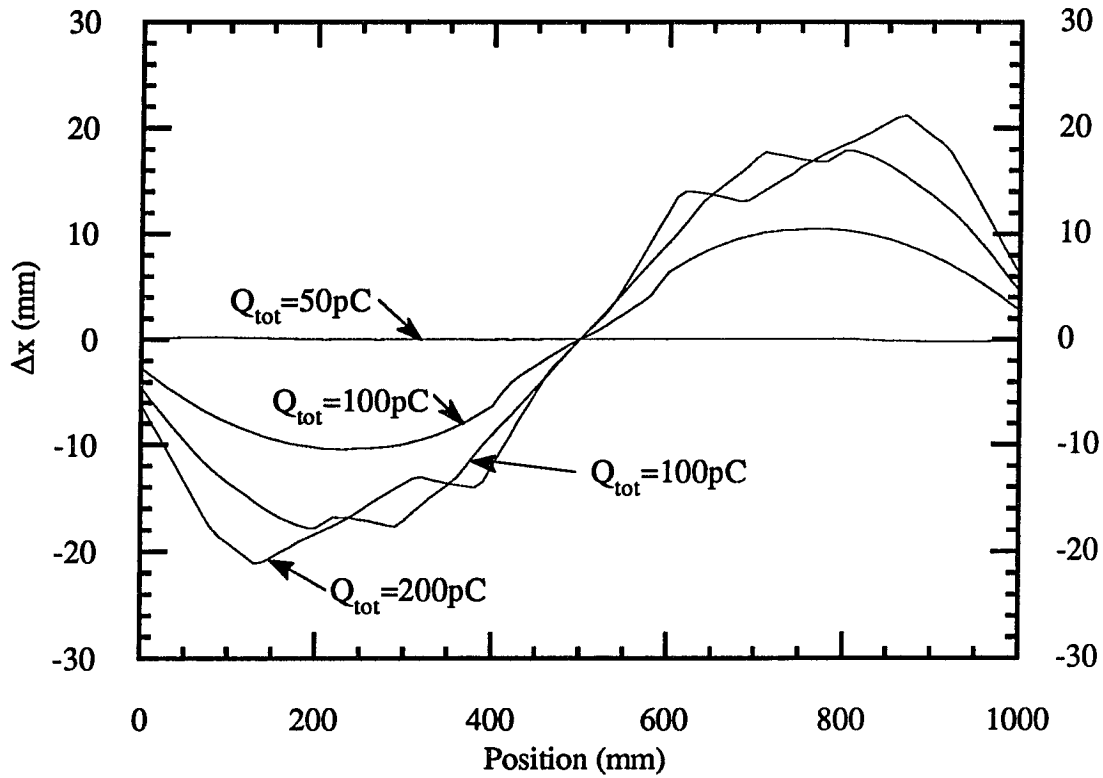


Fig 4.4 Effects of non-linearity of preamps on position calculation both preamps are assumed to have the same nonlinearity.  $Q_{tot}$  is the total charge input to the the two preamps.

The following two figures demonstrate the effects of error in the input impedance of the preamps. Figure 4.5 shows the effects if the impedance used in the calculations is different from the actual. Figure 4.6 shows the error that comes from the preamps having different impedances.

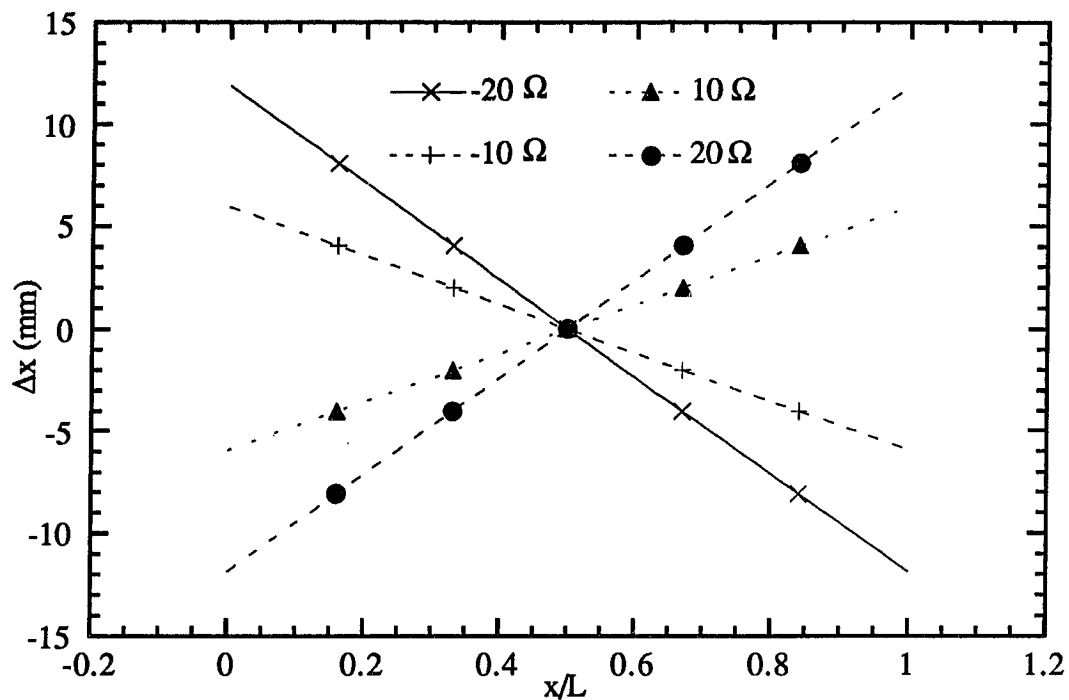


Fig 4.5 Error in position measurement due to incorrect input impedance of both preamps.

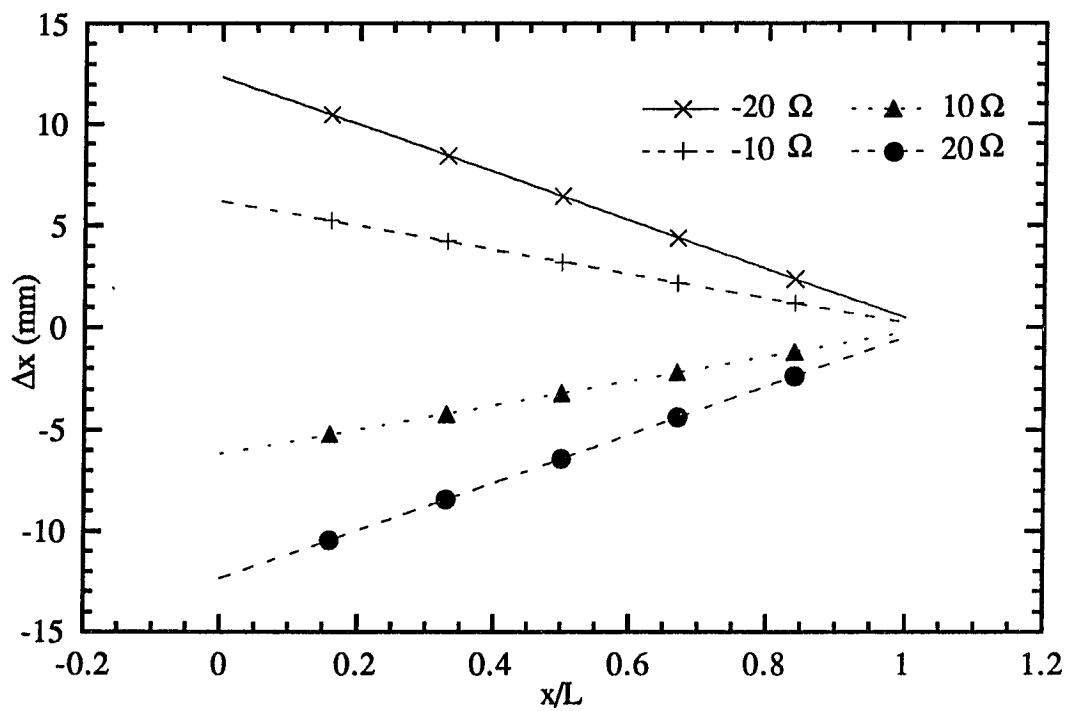


Fig. 4.6 Position error due to variation of the input impedance of one of the preamps.

#### **4.2.2. Design of Preamp Board**

In the design the signal ground and power ground have been separated so that we can connect them, leave them separate, or capacitively couple them. In the test set up, I have found that the best ground comes when the two are connected. There are also a pair of diodes which prevent damage to the preamps in case the power is connected incorrectly.

Figures 4.7 and 4.8 show the front and back of the preamp board. The front of the board distributes the signals while the back supplies power and ground. The signals come in the top of the board and flow down. The resistor and the input capacitor reside at the very top. The column of 10 holes are for the sockets that will hold the preamps. The use of sockets allows easy replacement of a faulty preamp without the need to remove the board. There are four outputs from the preamp: 2 AC outputs and 2 DC. The AC outputs are used to drive a differential signal through the twisted pair ribbon cable. This gives twice the signal of a single ended preamp as well as common mode rejection. The DC outputs are not used in this design. The AC outputs lead to a standard 2 x 17 header. From this point the signal is taken to the receiver board.

#### **4.2.3. Requirements**

The preamps draw about 50 mA of current from each the positive and negative supplies. It was also found helpful to wrap the chips in copper tape and ground them to power ground. This helps with noise pickup due to stray EMF. Power and ground for the chamber is supplied through a 2 x 8 header on the lower left. At this point we supply a test signal, crate/power ground, and  $\pm 11V$ .

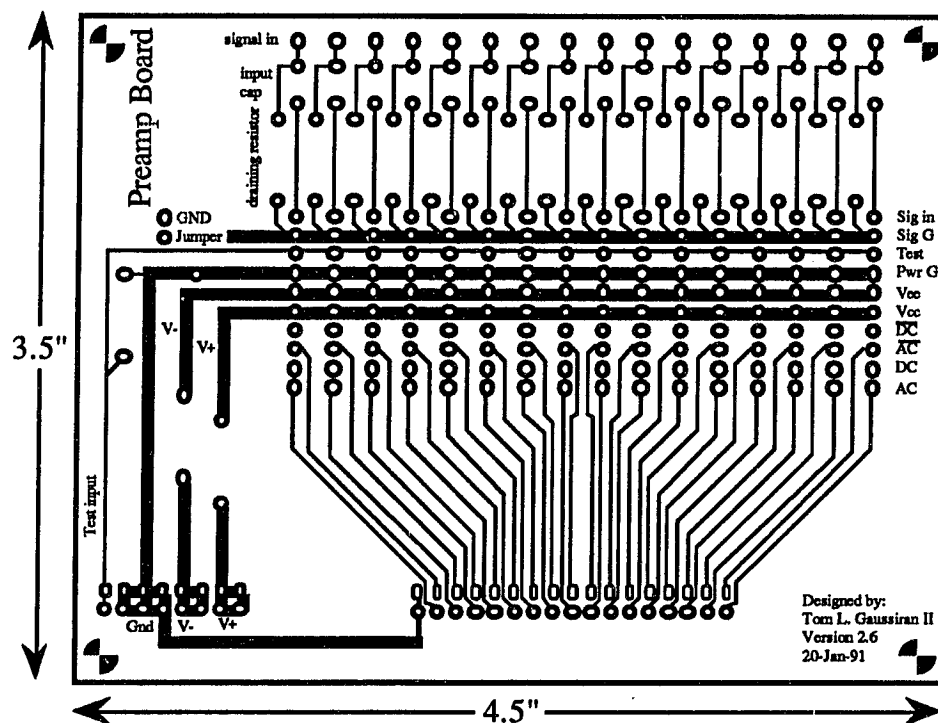


Fig 4.7 Front of the preamp board.

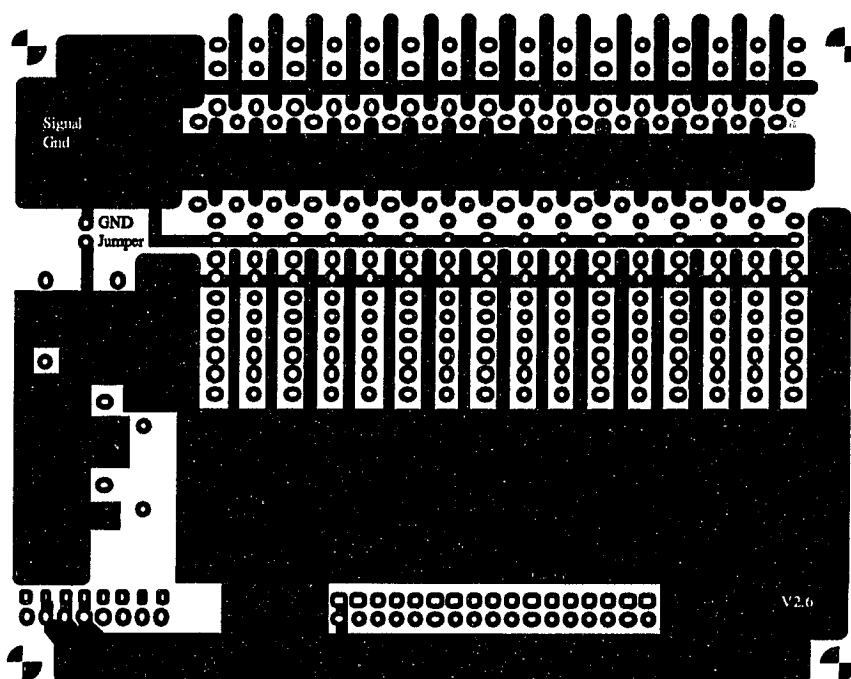


Fig 4.8 Back of the preamp board.



### **4.3. Receiving Board**

#### **4.3.1. Introduction**

This board has several functions. From this point the signal can be split to three different places. The more important part of the signal, for charge division, will go through the  $R_f$  resistor which leads to the ADC. The ADC signal comes from the resistor or jumper and then through a decoupling capacitor and finally out to the ADC. The second place for the charge to go is through  $R_t$  which is the resistor that is used to pick off the signal to the TDC. The TDC signal is added to the signal from the opposite side of the same wire by passive addition with resistors. If there is an excess of charge, we can put the excess charge of the input into a resistor ( $R_d$ ) to ground to keep the signal in the range of the other two components.

#### **4.3.2. Design**

The preamps are designed to drive a  $100\ \Omega$  load while the FERA's have a  $50\ \Omega$  input. The signal after entering the board goes first to a 2:1 transformer which brings the signal from differential to single ended and matches the  $100\ \Omega$  impedance to the  $50\ \Omega$  of the FERA.

The discriminator chip is the LeCroy MVL407. This chip has a slew rate of a few nsec which makes it excellent for timing purposes. The MVL407 is actually four separate discriminators on a single chip. The threshold voltage can be set independently for each channel but in this design all the thresholds are tied together and are set externally. The externally set threshold voltage is divided on the board. This means that noise pickup from the power supply is not as important since the noise is divided along with the threshold. The leading edge of this output is the stop timing signal for the TDC. The start for the TDC

will be taken from the scintillator array. The minimum discrimination voltage is 1 mV in order to have good timing resolution the signal must be well above this point.

The TDC signal then goes to the rear header. The cable can be pulled out the back or there is room left to bring it out the front. On the initial design there is also the ability to put pull down resistors into the circuit. The FERET system is ECL (emitter coupled logic) so it does not need these pulldown resistors and has been taken out of the final design. It is useful in the test boards since ECL signals would need a special adapter to be seen with a scope. The discriminated signal then goes out twisted pair ribbon cable which is 100  $\Omega$  to the TDC.

#### 4.3.3. Component Choices

It will be important when choosing the components for the receiver board that the resistances have an equivalent input impedance of 50  $\Omega$  as well as achieving the division required. This can be written as:

$$\frac{R_d (R_t + R_a) (R_f + 50\Omega)}{R_d (R_t + R_a) + (R_f + 50\Omega) (R_d + R_t + R_a)} = 50 \Omega \quad \text{Eq 4.1}$$

The ratios going to each of the three places can also be written as follows:

$$\frac{I_f}{I_o} = \frac{R_d}{R_d + R_{eq}} \frac{R_{eq}}{R_f + 50\Omega} \quad \text{Eq 4.2}$$

$$\frac{I_t}{I_o} = \frac{R_d}{R_d + R_{eq}} \frac{R_{eq}}{R_a + R_t} \quad \text{Eq 4.3}$$

$$V_t = I_o 50 \Omega \quad \text{Eq 4.4}$$

$$\frac{I_d}{I_o} = \frac{R_{eq}}{R_{eq} + R_d} \quad \text{Eq 4.5}$$

Where we have used the definition:

$$R_{eq} = \frac{(R_s + R_t)(R_f + 50\Omega)}{R_s + R_t + R_f + 50\Omega} \quad \text{Eq 4.6}$$

As well as the definition  $I_0$  being the input current to the receiver board.

We can now make a table of reasonable values for  $R_t$ ,  $R_a$ ,  $R_d$ , and  $R_f$  for different amounts of charge at the sense wires. The values of Table 4.1 try to keep the charge to the digitizers in the range of the respective components, and gives some attention to crosstalk between the two ends of a wire through the passive addition circuit.

| #e <sup>-</sup><br>From<br>Chamber | Q <sub>tot</sub><br>#e <sup>-</sup> | Q <sub>tot</sub><br>pC | R <sub>f</sub><br>Ω | R <sub>t</sub><br>Ω | R <sub>a</sub><br>Ω | R <sub>d</sub><br>Ω | Q <sub>adc</sub><br>pC | Q <sub>tdc</sub><br>pC | Q <sub>d</sub><br>nC | V <sub>tdc</sub><br>mV |
|------------------------------------|-------------------------------------|------------------------|---------------------|---------------------|---------------------|---------------------|------------------------|------------------------|----------------------|------------------------|
| 2 x 10 <sup>7</sup>                | 10 <sup>9</sup>                     | 160                    | 30                  | 121                 | 12.1                | ∞                   | 100                    | 60                     | 0                    | 4                      |
| 5 x 10 <sup>7</sup>                | 2.5 x 10 <sup>9</sup>               | 400                    | 50                  | 90.9                | 9.1                 | ∞                   | 200                    | 200                    | 0                    | 10                     |
| 1 x 10 <sup>8</sup>                | 5 x 10 <sup>9</sup>                 | 800                    | 150                 | 136                 | 14                  | 100                 | 200                    | 200                    | .4                   | 20                     |
| 2 x 10 <sup>8</sup>                | 10 <sup>10</sup>                    | 1600                   | 350                 | 364                 | 36                  | 66                  | 200                    | 200                    | 1.2                  | 40                     |
| 5 x 10 <sup>8</sup>                | 2.5 x 10 <sup>10</sup>              | 4000                   | 950                 | 909                 | 91                  | 55                  | 200                    | 200                    | 3.6                  | 100                    |
| 1 x 10 <sup>9</sup>                | 5 x 10 <sup>10</sup>                | 8000                   | 2K                  | 1.8K                | 182                 | 52.6                | 200                    | 200                    | 7.6                  | 200                    |
| 2 x 10 <sup>9</sup>                | 10 <sup>11</sup>                    | 16000                  | 4K                  | 3.6K                | 364                 | 51                  | 200                    | 200                    | 15.6                 | 400                    |
| 5 x 10 <sup>9</sup>                | 2.5 x 10 <sup>11</sup>              | 40000                  | 9.1K                | 9.1K                | 910                 | 50.5                | 200                    | 200                    | 39.6                 | 1000                   |

Table 4.1 Suggested resistance values for various input values to the receiver board. Note that the preamp saturates at inputs above 50 pC or 3 x 10<sup>8</sup> e<sup>-</sup>

#### 4.4. Digitizers

Charge division requires 2 ADC channels for every wire. Fast digitization is accomplished by using the LeCroy FERA (Fast Encoding and Readout ADC) system. The fast digitization time and buffer transfer time (20μs) of the FERA systems make it uniquely

suited to the LAMPF beam structure of 120 Hz at 10% duty. The FERAs have 11 bits however some of this is taken up in overhead. Due to the overhead instead of the maximum channel being 2048 it is 1919 with the pedestal usually near 60 channels. Each ADC channel represents 0.25 pC this gives them a full range of 500 pC.

There were two slight modifications which had to be made to the FERAs before they were used. The first had to do with removing pulldown resistors in all but the last module used. This has to be done so that the distributed signal from the FERA controller is terminated properly. The other change was to increase the charge injection. It was found that the default charge injection was too low. This increase was accomplished by adjusting a variable resistor inside the FERA.

## **Chapter 5: Results**

### **5.1. Introduction**

The test chamber was constructed so that the electronics could be tested. It also provided insight into the techniques for stringing wires in the cylindrical chamber. Most of the work for this thesis has gone into the construction and testing of the test chamber. From this chamber we learned how to string wires, fix broken wires, connect preamp boards to the chamber, and techniques for eliminating ground loops. Most importantly, we demonstrated that charge division can work at the desired level of precision.

We tried to be methodical in the examination of the different stages of the electronics. The naive belief that the chamber could be turned on, the electronics hooked up, and expect 1% z resolution was quickly put aside.

A large part of the effort of this research has actually been spent trying to reduce noise. One of the most difficult tasks is eliminating ground loops. The one guiding principle used was to make the grounds come from a central branch. To do this the two crates were grounded together. From the crates, the ground for the chamber was pulled. It is important to note that the chamber not be connected with the ground in any other places. The chamber is electrically isolated on a wooden desk and the cylindrical chamber will have to be isolated from the ground by some insulating material. The the ground for the preamp board comes from the power supplies which share a common ground with the crates.

### **5.2. Design**

The test chamber is square and constructed of aluminum. The aluminum plates that make up the walls are butt jointed and are made air tight by with rubber gaskets. The windows of the chamber are covered with aluminized mylar. This window allows particles

to pass through easily, is airtight and is a good ground plane against noise. The endcaps of the chamber are drilled with the pattern shown in figure 5.1.

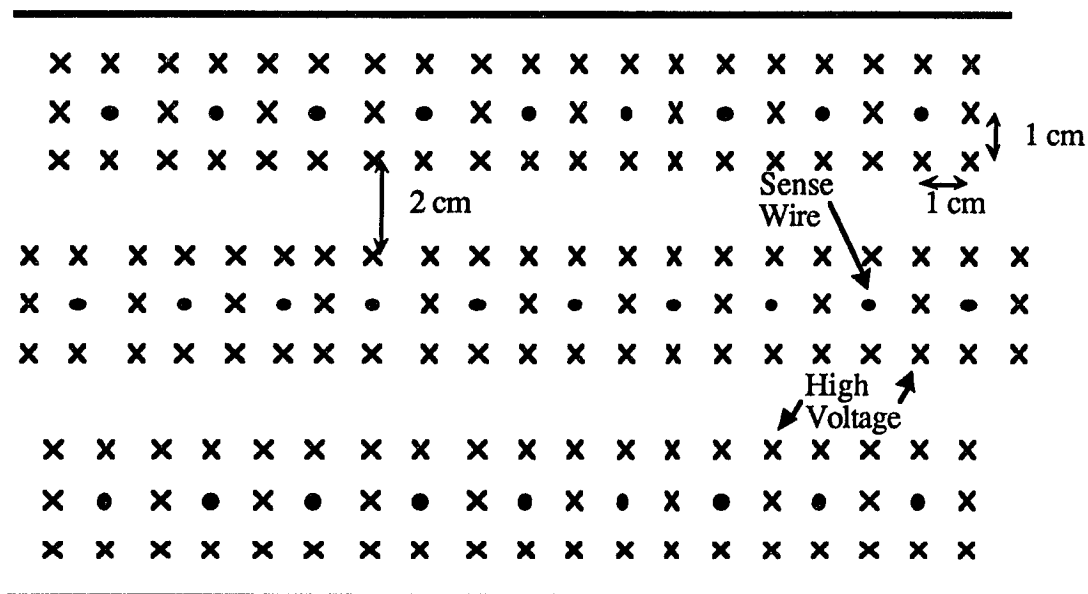


Fig 5.1 Present test chamber hole pattern found in the endcaps.

The solid circles are the sense wires and the x's are the high voltage wires. The spacing between wires is 1 cm. The chamber has been fully wired but only the center region is active. There are five sense wires connected to preamps on the top and bottom layers and six in the center. The active region consists of the wires that are in front of the window.

### 5.3. Single Wire Measurements

The question of precision is difficult to address. Preliminary tests used a signal from a pulser shaped to look like a chamber pulse to test the electronics. A meter stick was strung with stableohm wire across its length then a preamp was attached to either side. It was possible to clip the output of the pulser along the length of the wire and test the electronics. The “problem” with this test is that the pulser is very quiet and the signal can be made very

large without affecting the noise. Perhaps the most important problem with this test is that the size of the pulses is constant.

Figure 5.2 shows the difference between measured and calculated position for a measurement with a 100 pC input. There is evidence for non-linear response (Fig 4.4) and a difference between gains at the two ends (Fig 4.2). The error bars are an estimate as to the ability to accurately measure the position along the wire.

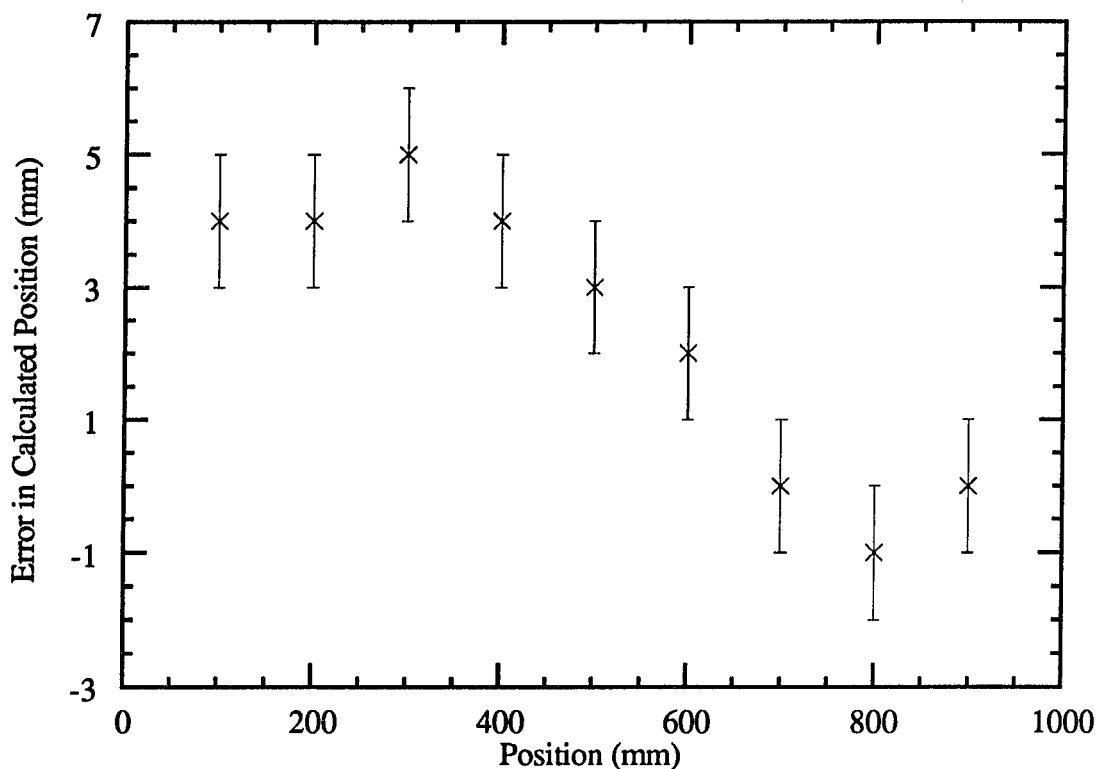


Fig 5.2 Position Resolution

Now we can look at the position measurement. It is the position as calculated with a pulser clipped at 900 mm on a test wire of 1 meter. The lower axis is in mm and we can see the we obtain a FWHM of only a  $\approx 7$  mm.

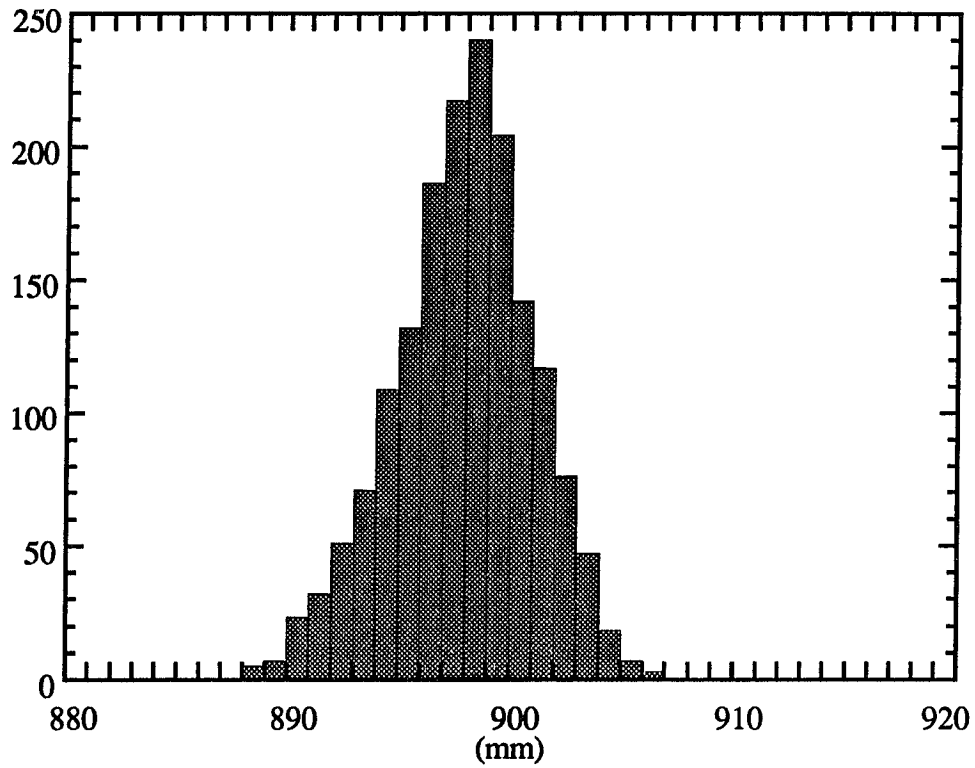


Fig 5.3 Position Calculation

#### **5.4. Test Chamber Measurements**

The first test chamber measurements were done with sources but the precision of our results were limited by multiple scattering. In our current setup, we trigger on high energy cosmic rays to obtain minimum ionizing muons. The setup is shown in figure 5.4.



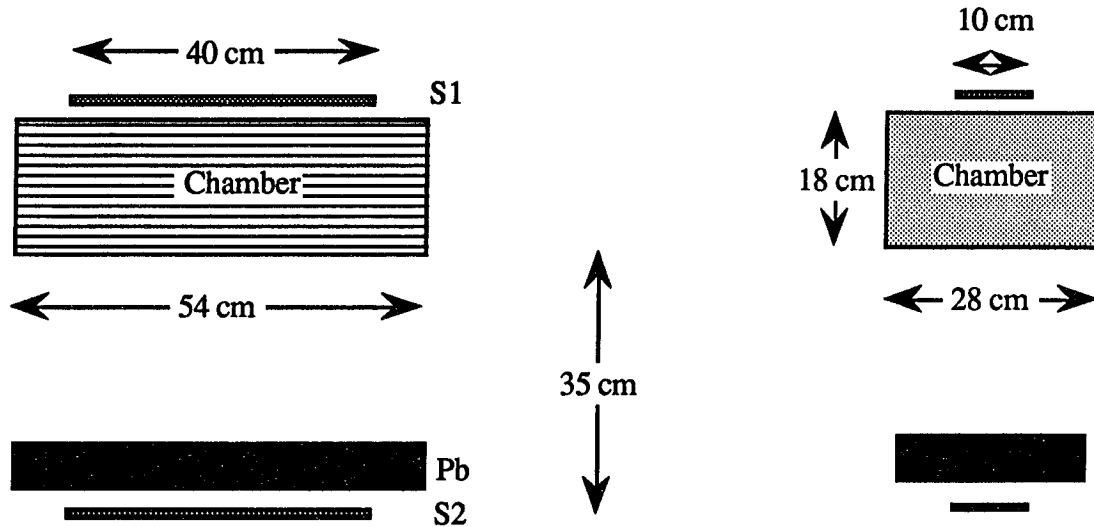


Fig 5.4 Side view and end view of test chamber as used with gating scintillators.

To evaluate the performance of the test chamber we will look at efficiencies and residuals. Efficiencies were defined in two ways. In the first, we use the fraction of triggers for which each plane of wires was hit. A plane is hit if at least one wire fires, that is, if the total charge deposited on the wires is above a threshold. In our testing we have used 1 pC for this cut, which is located in the histograms at 200 channels. Figure 5.5 shows a typical ADC spectra from a single wire. Note that the signal is well separated from the noise.

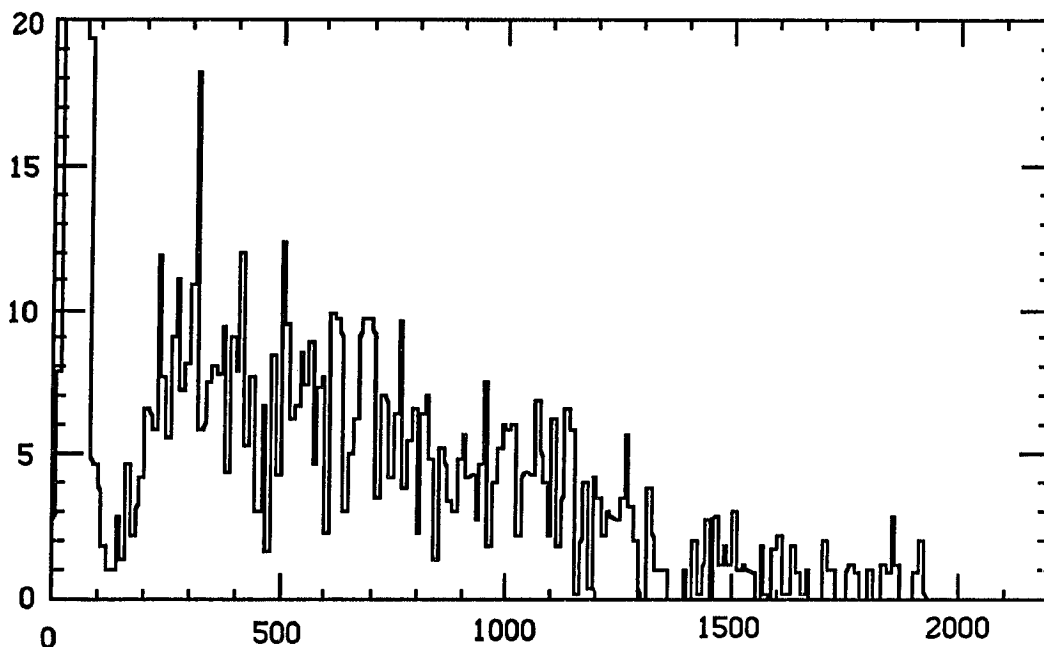


Fig 5.5 Typical FERA spectra from a single wire in the test chamber. Run with 70% Argon 30% Isobutane

It is possible to define efficiency in many ways, the most important would be if the scintillators fired then did one wire fire in every plane in the chamber. Figure 5.6 shows a histogram of the corresponding multiplicity. If the chamber were working perfectly then one would expect that all the counts would be in channel 3. This excludes the accidentals in the scintillators which give counts in channel 0. One notes that there are some events in which the chamber only fires 1 or 2 wires, this corresponds to inefficiencies in the chamber.

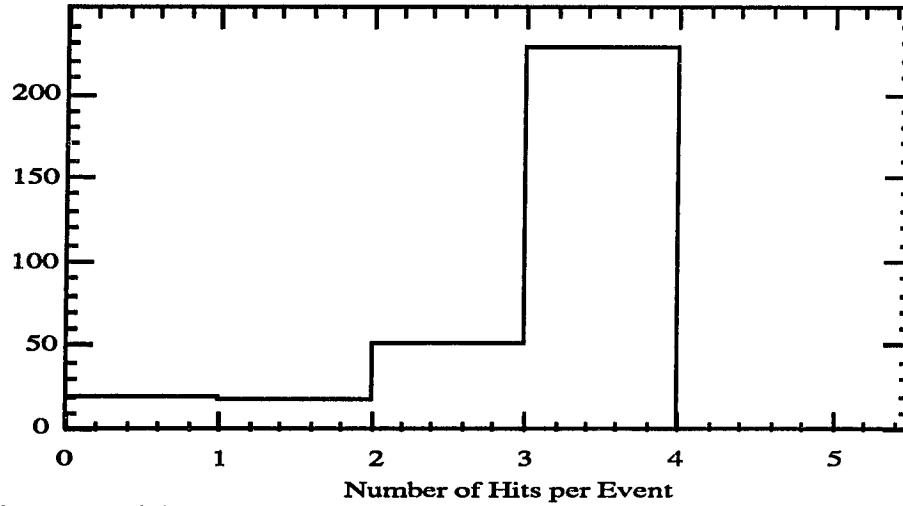


Fig 5.6 Histogram of the number of planes to fire in the chamber per scintillator event

Another way of defining the efficiency involves looking at one plane and using the other two planes to define an event. One can express this efficiency as  $\epsilon_1 = \frac{p_1 \cdot p_2 \cdot p_3}{p_2 \cdot p_3}$  where  $p_i$  represents one wire firing in plane  $i$ . Using this definition we find that the efficiency per plane is approximately 95%.

In order to calculate the residual one finds the wire that was hit in each layer. If one and only one wire was hit in each plane then a residual is calculated. A hit is defined as being when the sum of the two sides of the wire greater than a minimum value and there are no overflows in any single channel. For our calculations the minimum sum was 200 channels or 50 pC. With the information of the charge deposited on each end the  $z$ -position in the wire is calculated. Finally, take the average position of the outer two layers and subtract the inner layer position. Assuming that one has a particle that goes through and only ionizes the gas and does not scatter, this residual should give 0. One can write this equation as follows, where we use  $z_1$ ,  $z_2$ , and  $z_3$  to be the position on the wire for each plane.

$$\text{residual} = \frac{1}{2} (z_1 + z_3) - z_2 \quad \text{Eq. 6.1}$$

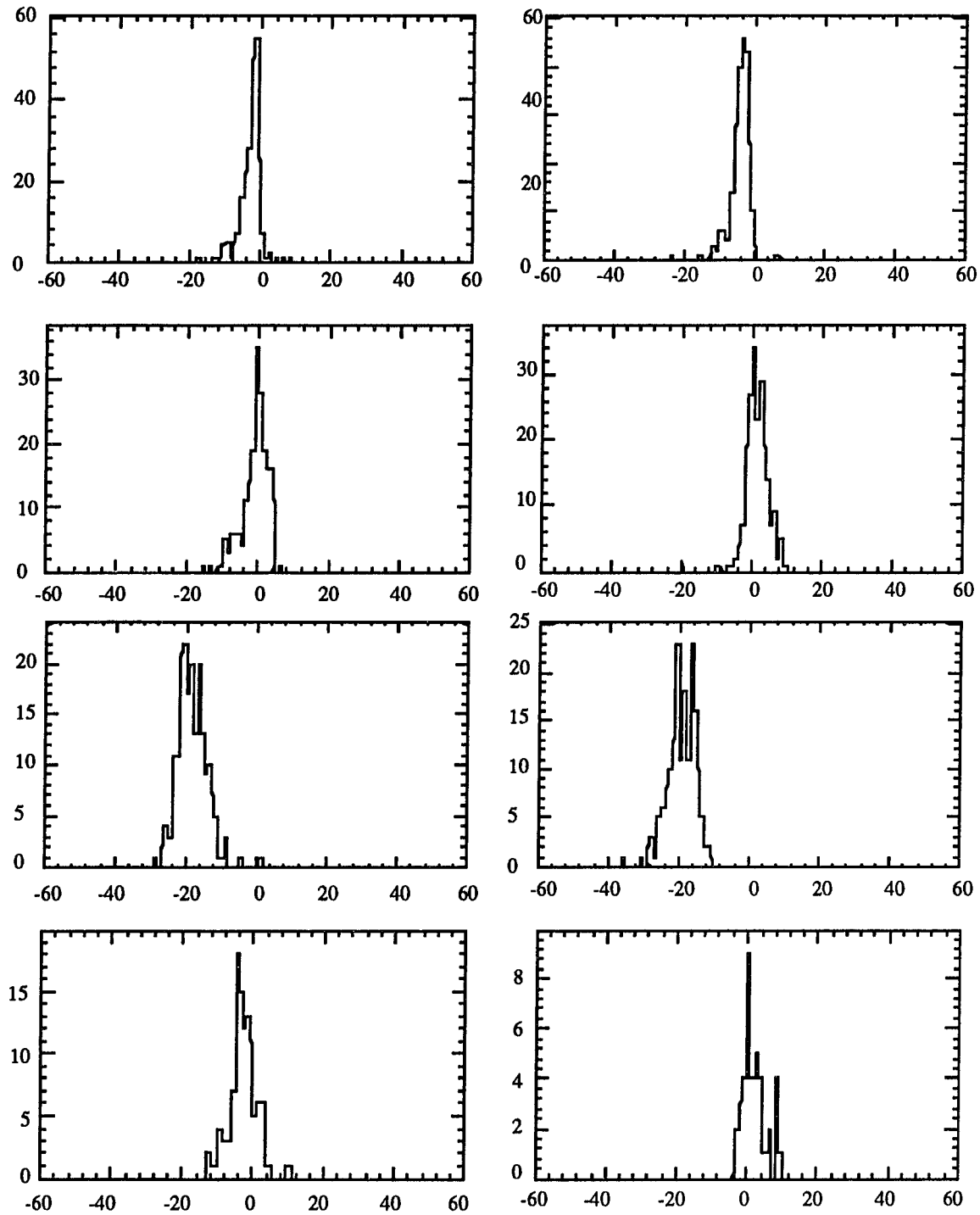


Fig 5.7 Residual for different triples of wires in the test chamber. The lower axis is in mm. Note that two of the sets of wires has a residual which is offset from zero by two cm.

Although the residuals are fairly sharp (5-10 mm FWHM), two are offset by 2 cm. The sense wires pass through a narrow copper tube which extends 4 cm into the chamber beyond the point where the wire is crimped. Some of the wires may contact this tube somewhere along this length, shorting the resistive wire. We believe this condition is responsible for the offsets observed in the residual spectra.

It is interesting to compare the error in the charge measurement with the error in the position measurement to see if this is the limiting factor. The charge error at this point is approximately 14 channels FWHM with the  $Q_{\text{tot}}$  being about 1000 channels. This gives us a  $\frac{\Delta Q}{Q} = .014$  and therefore we would predict a  $\Delta x$  of 8 mm FWHM. The residuals in figure 5.7 are consistent with this value.

## **Chapter 6: Conclusions**

This thesis has tried to cover the development process of a drift chamber utilizing charge division. A program was written to help choose a suitable geometry as well as study drift chambers. Electronics were designed and built which have the capability of collecting the charge from a chamber, amplifying it, and then digitizing the signal. A test chamber was built which shares many of the properties of the cylindrical chamber. Finally, all of these components were assembled and were shown to work. The precision obtained of 3 mm is well below that needed by the experiment.

### **Improvements and Extensions**

The main topic which needs to be addressed in the immediate future is whether this offset can be eliminated. An idea for a way to do this without sacrificing supplies is to make the lower portion of the copper tube non-conducting. A possible way of accomplishing this is with a dip or a bathe which could insulate the inside of the copper yet not seal the tube.

A very important topic which was not addressed was the drift time measurement. The discriminators exist on the receiver board but they have not been used to calculate positions. It will be critical to the experiment to get this part of the electronics working.

Another topic that should be addressed is whether to use the FERA pedestal subtraction along with the zero suppression. This would considerably help the live time but it has been noticed that the zero point has some width to it. Therefore, one must be careful as to how to calculate this as well as how often it should be checked. For instance it may be possible that between spills, pedestal runs could occur and these values written back to the FERA.

## Appendix A: MWDC a users guide

This appendix contains an example of what a data input file for MWDC might look like. The numbers in bold correspond to an explanation which follows. All distances are in cm, all voltage are in Volts, magnetic fields are in kGauss. The radius is stated when speaking of the wire.

```

1   Drift with Magnetic Field
2   1,1,1,1,0,1,1,1,0,0
3   70,1.0
4   6,800
5   12,0.0,0.0
6   18, 2.0
7   0.0, 1.0, 0.0635, -3400.0
      1.0, 1.0, 0.0635, -3400.0
      0.0, 2.0, 0.01651, 000.0
      1.0, 2.0, 0.0635, -3400.0
      0.0, 3.0, 0.0635, -3400.0
      1.0, 3.0, 0.0635, -3400.0
      0.0, 5.0, 0.0635, -3300.0
      1.0, 5.0, 0.0635, -3300.0
      0.0, 6.0, 0.0635, -3300.0
      1.0, 6.0, 0.01651, 000.0
      0.0, 7.0, 0.0635, -3300.0
      1.0, 7.0, 0.0635, -3300.0
      0.0, 9.0, 0.0635, -3400.0
      1.0, 9.0, 0.0635, -3400.0
      1.0, 10.0, 0.0635, -3400.0
      0.0, 10.0, 0.01651, 000.0
      0.0, 11.0, 0.0635, -3400.0
      1.0, 11.0, 0.0635, -3400.0
      end
8   0.0
9   5,.25
10  1,450,.005
11  e-
12  0.003
13  321455,123679,908753,113419,345673
      457651,896573,908771,763549,356471
      786543,908765,132247,876453,786591
      987865,764533,657971,565789,654693
14  0.00,1.0,0.25,0.0,0.0
```

!Number of wires, cell size  
!x,y,r,v (cm,V)

!b0(kGauss)

! Ionizing particle momentum

! vx,vy,x0,y0,z0

1. Title of the simulation, attached to the output file saveit.out.
2. This is a where the options are set for the program to execute. A 1 means that that option is turned on and a 0 means it is turned off. These controls are in order.

- 1) Calculate track of ionizing particle
- 2) Calculate track of drift electrons
- 3) Write out the potential to FOR006
- 4) Write out ion track to FOR006
- 5) Write out drift tracks to FOR006
- 6) Write out drift tracks in xy format to FOR008
- 7) Write out signal information to FOR020

8) If set to 1 it uses the IMSL libraries. If IMSL is not available, set to 0 and MWDC uses internal routines. This can be a real speed improvement over the IMSL setting although some accuracy is lost since, for instance, instead of using spline fits it will just do a linear fit. At this time this is not entirely guaranteed since a few of the IMSL routines do not have replacement subroutines.

Also, these settings are fairly safe in that it will not accept controls that are incompatible for instance if it is not told to compute the tracks for the ionizing particle, yet it is told to compute the drift electrons tracks, it will not track these electrons since they were never formed.

3. % of gas that is Argon, pressure in atmospheres
4. Time between drift step, maximum drift time
5. Spacing between the front and the back of the chamber, voltage on the front wall, voltage on the back wall



6. The number of wires in the unit cell. This must match with the number in the list to follow, the unit cell size in cm.

7. The x coordinate, y coordinate, the radius of the wire, and the voltage of the wire

8. The magnetic field strength in kGauss

9. The number of cells to either side of the central one that the tracking will allow, the step size for dividing up the unit cell (in cm)

10. Number of ionizing particle tracks, maximum number of steps, and step size

11. The identity of the ionizing particle

12. Ionizing particle momentum

13. Random number seeds

14. The ionizing particles' momentum unit vectors  $p_x, p_y$ , and the starting position  $x, y, z$

## Appendix B: Jacobi Elliptic Functions

The problem of wires placed between two parallel conduction planes is solved in Morse and Feshbach. They find an analytic solution for the problem in which there is a grid of wires spaced a distance  $2b$  apart between two parallel plates held at ground which are a distance  $a$  apart and the wires are a distance  $x_0$  from the plate at  $x=0$ . In the following figure the dark solid lines are the foils of the chamber viewed with the wires coming up out of the page. The wires are the  $+$  between the solid lines and they are repeated up and down every  $2b$ . If we set the right plane to be at  $x=0$  then the wires are located at  $z = x_0 + i 2nb$  for  $n=0, \pm 1, \pm 2, \dots$ . There are image charges of opposite sign at  $z = -x_0 + 2ma + i 2nb$  for  $m, n=0, \pm 1, \pm 2, \dots$  and image charges of the same sign for  $z = x_0 + 2ma + i 2nb$  for  $n=0, \pm 1, \pm 2, \dots$  and  $m = \pm 1, \pm 2, \dots$

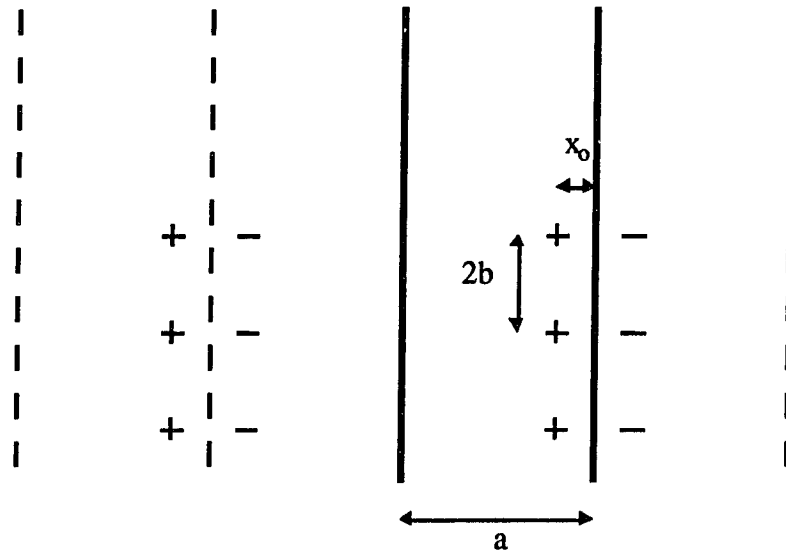


Fig B.1 Geometry used to compute potential

There are three main Jacobi Elliptic functions:  $\text{sn}(u, k)$ ,  $\text{cn}(u, k)$ , and  $\text{dn}(u, k)$ . These functions have the useful property of being doubly periodic in the complex plane. The

second argument  $k$  is usually assumed and not written. This double periodicity means that along both the real and imaginary axis there are alternating poles and zeros. There are simple poles for the three functions at  $2mK + i(2n+1)K'$ . The simple zeroes are located at  $2mK + 2i nK'$  for  $sn$ , at  $(2m+1)K + 2i nK'$  for  $cn$ , and at  $(2m+1)K + i(2n+1)K'$  for  $dn$  for integers  $m, n$ . The Jacobi elliptic integral  $K$  is the quarter periodicity of the Jacobi elliptic functions. There are five parameters that can be given to identify the Jacobi elliptic function namely  $K, K', k, k', \frac{K}{K'}$ . These quantities are not independent and once one is given the rest are determined. The quantities are related to the geometry in the following simple way  $K/K' = a/b$  where  $a$  is the foil separation and  $b$  is the half the distance between wires. The parameters  $k$  and  $k'$  are the same parameters as for the Jacobi Elliptic Integrals which are  $K$  and  $K'$ . Where we have used the definition  $K' = K(k')$ . Also, we have the relationship that  $k^2 + k'^2 = 1$ .

The positive (negative) poles are then used to represent positive (negative) charge on the wires. They claim that since this function has the proper boundary conditions and is a solution to Poisson's equations then this is the only solution. The important boundary conditions to notice are  $F(0, y) = F(a, y) = 0$ . It should also have poles at  $z = x_0 + 2na + 2i mb$  and zeroes at  $z = -x_0 + 2na + 2i mb$ .

There are several relations which one needs to check these limits. These functions are can be related to more familiar functions to which they reduce in the following limits. For instance for  $k \approx 1$  we have:

$$sn(u) \approx \tanh u$$

$$cn(u) \approx \operatorname{sech} u$$

$$dn(u) \approx \operatorname{sech} u$$

And when  $k \approx 0$  we have:

$$sn(u) \approx \sin(u)$$

$$cn(u) \approx \cos(u).$$

$$dn(u) \approx 1$$

Several equivalent definitions for these functions exists. One of the most useful of these is:

$$\begin{aligned} \operatorname{sn}^{-1}(x,k) &= \int_0^x \frac{dx}{\sqrt{(1-x^2)(1-k^2x^2)}} & \operatorname{cn}^{-1}(x,k) &= \int_x^1 \frac{dx}{\sqrt{(1-x^2)(1+k^2-k^2x^2)}} \\ \operatorname{dn}^{-1}(x,k) &= \int_x^1 \frac{dx}{\sqrt{(1-x^2)(x^2+k^2-1)}} \end{aligned}$$

There are some other properties that are similar to circular functions from whom they take their symbols, such as:

$$\begin{aligned} \operatorname{sn}^2(u,k) + \operatorname{cn}^2(u,k) &= 1 \\ k^2 \operatorname{sn}^2(u,k) + \operatorname{dn}^2(u,k) &= 1 \\ \operatorname{sn}(0) &= 0 & \operatorname{cn}(0) &= 1 & \operatorname{dn}(0) &= 1 \\ \operatorname{sn}(-u) &= -\operatorname{sn}(u) & \operatorname{cn}(-u) &= \operatorname{cn}(u) & \operatorname{dn}(-u) &= \operatorname{dn}(u) \\ \operatorname{sn}(u+v) &= \frac{\operatorname{sn}(u) \operatorname{cn}(v) \operatorname{dn}(v) + \operatorname{cn}(u) \operatorname{sn}(v) \operatorname{dn}(u)}{1 - k^2 \operatorname{sn}^2(u) \operatorname{sn}^2(v)} \\ \operatorname{cn}(u+v) &= \frac{\operatorname{cn}(u) \operatorname{cn}(v) - \operatorname{sn}(u) \operatorname{sn}(v) \operatorname{dn}(v)}{1 - k^2 \operatorname{sn}^2(u) \operatorname{sn}^2(v)} \\ \operatorname{dn}(u+v) &= \frac{\operatorname{dn}(u) \operatorname{dn}(v) - k^2 \operatorname{sn}(u) \operatorname{sn}(v) \operatorname{cn}(u) \operatorname{cn}(v)}{1 - k^2 \operatorname{sn}^2(u) \operatorname{sn}^2(v)} \end{aligned}$$

The other piece of information that will be needed to implement the Morse and Feshbach solution is how to break the Jacobi Elliptic functions into real and imaginary parts

when you have complex arguments. For this it is convenient to make the following definitions:

$$\begin{aligned} s &= \text{sn}(x, k) & s_1 &= \text{sn}(y, k') \\ c &= \text{cn}(x, k) & c_1 &= \text{cn}(y, k') \\ d &= \text{dn}(x, k) & d_1 &= \text{dn}(y, k') \end{aligned}$$

Then we can write the complex value as follows:

$$\begin{aligned} \text{sn}(x+iy) &= \frac{s d_1 + i c d s_1 c_1}{c_1^2 + k^2 s^2 s_1^2} \\ \text{cn}(x+iy) &= \frac{c c_1 - i s d s_1 d_1}{c_1^2 + k^2 s^2 s_1^2} \\ \text{dn}(x+iy) &= \frac{d c_1 d_1 - i k^2 s c s_1}{c_1^2 + k^2 s^2 s_1^2} \end{aligned}$$

Morse and Feshbach's solution then looks like

$$F = 2q\text{Re} \ln \left[ \frac{\frac{\text{cn}(2\theta)}{\text{sn}(2\theta)} - \frac{(csc_1 d_1 - s c d^2 s_1^2 c_1 d_1) - i (c^2 d c_1^2 s_1 + s^2 d d_1^2 s_1)}{(s d_1)^2 + (c d s_1 c_1)^2}}{\frac{\text{cn}(2\theta)}{\text{sn}(2\theta)} - \frac{\text{cn}(\theta)}{\text{sn}(\theta)}} \right]$$

Finally, we can take the real part of this; and, after making the following substitutions, we obtain a much simpler looking equation:

$$\begin{aligned} cs_2 &= \frac{\text{cn}(2Kx_0/a)}{\text{sn}(2Kx_0/a)} & cs_1 &= \frac{\text{cn}(Kx_0/a)}{\text{sn}(Kx_0/a)} \\ \text{and } csr &= \frac{(csc_1 d_1 - s c d^2 s_1^2 c_1 d_1)}{(s d_1)^2 + (c d s_1 c_1)^2} \end{aligned}$$

$$cs_i = \frac{i(c^2dc_1^2s_1 + s^2dd_1^2s_1)}{(sd_1)^2 + (cds_1c_1)^2}$$

$$F = q \ln \left[ \frac{(cs_2 - csr)^2 + cs_i^2}{(cs_2 - cs_1)^2} \right]$$

There is also a simple and fast way to calculate the Jacobi elliptic functions numerically using the Arithmetic-Geometric Mean. This method can be found in Numerical Recipes [12] on pg 189.

### Appendix C: Cylindrical Chamber Construction

The chamber consist of three major parts: the endplates, walls, and the wires. The chamber is cylindrical, the top and bottom are called the endplates and are constructed of Aluminum. The walls are made of a carbon fiber in an epoxy matrix covered with aluminized mylar

#### EndPlates

The endplates are extremely important in that their precision will determine the precision achieved radially. When all the wires are in place, the endcaps will be under a great deal of force (about 500kg-wt). To prevent warping due to this tension, 1 1/4" Aluminum jig plate was used. A close inspection of the hole pattern would show the following:

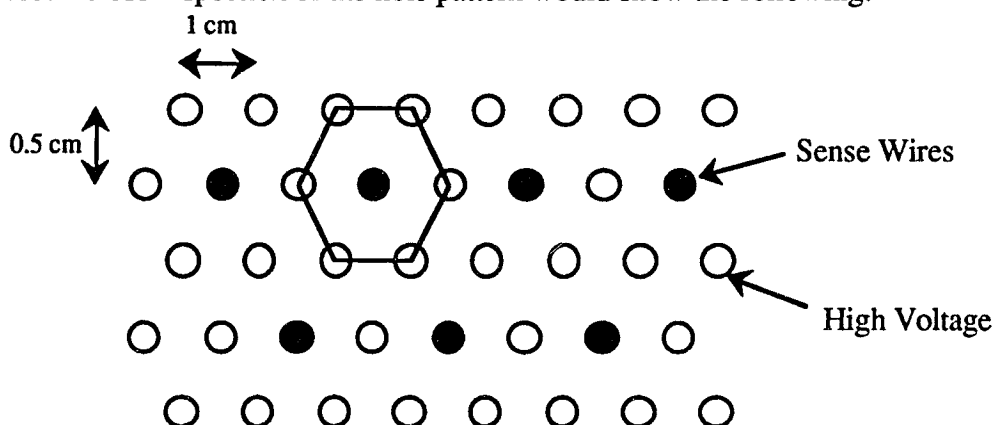


Fig C.2 Cylindrical chamber design

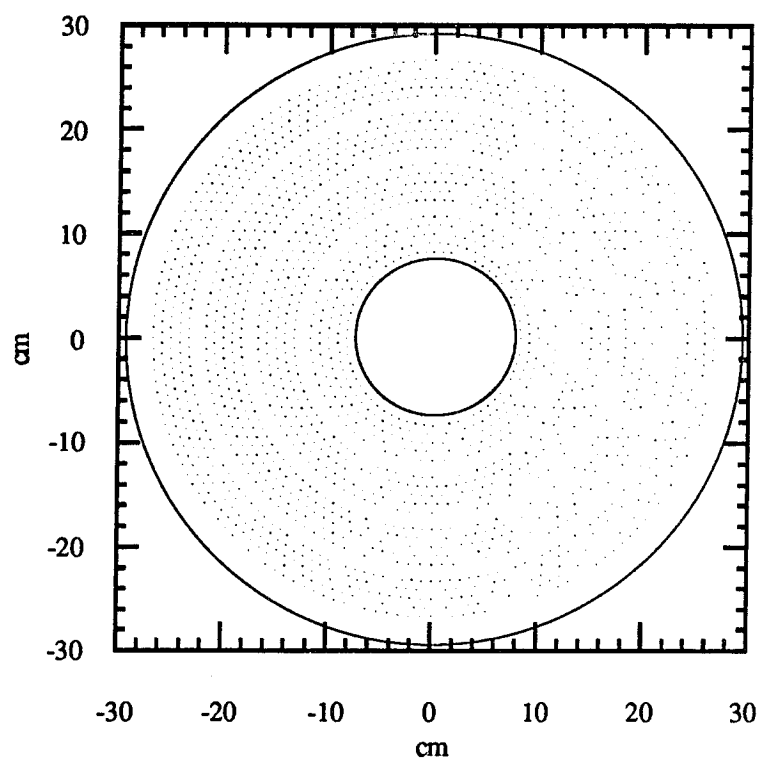


Fig C.2 Endcap for cylindrical drift chamber

The plate was precision drilled with 2240 - 126 mil holes into which the plastic feedthrus will fit.

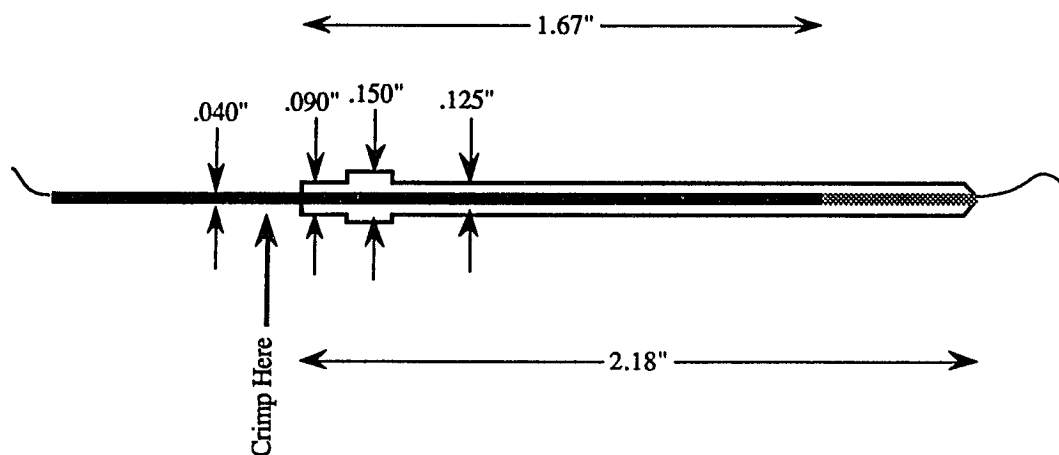


Fig C.3 Plastic feedthru, copper tube and wire



These holes are arranged in 4 layers with 5 rows in each layer. The spacing between each row is 0.5 cm and the distance between holes in a row is about 1 cm but as stated before the outer rows of a given layer have a wider separation than the inner one to keep the angular spacing constant.

The number of sense wires were chosen so that the inner layer can be equipped with 4 preamp boards each having 16 channels. The second layer takes 6 boards, the third 8 boards, and the outer most layer has 10 preamp boards. This is for a single side of the chamber and the other side needs an equal number of boards.

Each endplate has holes for 4 Swagelok connectors for 3/8" tubing to bring the gas in and out. There are drilled and tapped holes which will be used to attach a stand onto which the preamp boards will be mounted. Finally, there are also holes at the edges to attach handholds and supports. There are two 4 mm deep grooves cut into each endplate for the inner and outer cylinder .

### **Outer Walls**

The walls of the chamber are made of carbon fiber. This material was chosen because it is both strong and light. Fortunately, the group from the University of Houston working on the Mega project had some practice with making these carbon fiber cylinder and Kathleen Johnston taught us the following way of constructing them.

The cylinder was built over a collapsible mandril. The mandril was made so that after the carbon fiber has hardened the mandril could be removed, however until that time it must be a rigid right cylinder. The method we used was a modified version of what the group at the University of Texas designed. Starting from the inside we have a rod of cold rolled steel. Over this were fit several (4) sleeves which slide down the rod and were evenly spaced along it. Onto these sleeves a pair of aluminum half moons were bolted. The half

moons or ribs were cut so that they would not touch each other or the inner rod. This was very important to assure that they were removable when then were unbolted. Over the ribs were finally placed two rolled pieces of aluminum. A few hose clamps were placed on this outer shell and were pulled tight. The shells should not butt into each other since the inner layer of mylar will shrink and it will not be possible to remove them.

Onto this mandril we can started making our cylinder. This began by spiraling 10 mil mylar over the aluminum. The mylar was pulled very tight as it was wrapped on, and as one goes down the cylinder the hose clamps are removed. Kapton tape secures the mylar from unspiraling. The first layer of mylar gives a nice surface for the rest of the cylinder to be laid down onto and holds the shell of the mandril onto the ribs. Once this was secured at either end, followed the same spiraling procedure but with aluminized mylar.

Next, start placing layers of carbon fiber. The carbon fiber was actually already impregnated with an epoxy so that after curing it becomes rigid and very strong. The fibers were first laid with their strands along the long axis of the cylinder. Then four more layers were put down by spiral wrapping them in alternating directions. This crossing of the carbon fibers matrix lends strength to the structure. After this another spiral wrap of aluminized mylar was applied.

It was then wrapped with plain mylar again. This final wrapping of mylar shrinks on heating and presses the aluminized mylar into the epoxy matrix. The cylinder was placed in a large oven and baked at 250° F for 7 hours. During this time the outer layer of mylar shrinks and pulls the carbon fiber tightly onto the walls of the mandril and pressing the different layers into each other.

A machine shop cut the length from 48 in to the 42.1 in needed. The carbon fiber is a very abrasive material and will dull a normal blade quickly. We found that a carbide tipped

blade will cut nicely and leave a clean smooth surface. It is also a good idea when cutting the cylinder to score the outer mylar with a fine toothed blade. It is very important to leave the outer layer of mylar in place otherwise the outer coating of aluminum will rub off.

Now the mandril can be disassembled and the plain mylar taken off. The overlap of the aluminized mylar should be cut away. The aluminized mylar will be connected electrically with the endcaps and grounded making an effective shield.

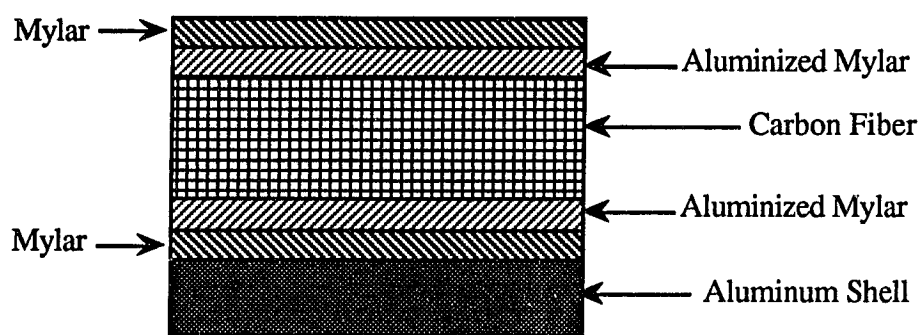


Fig C 4 Layers of cylinder in cross section

### Stringing wires

In stringing the drift chamber several different things are required. First, the wire must not slip or break once it is in place. If it does break, it should be easy to replace. It is also necessary to be sealed gas tight and have the wires be electrically isolated from the chamber. We used a technique for doing this that was adapted from the Mega chamber which is being built at the University of Houston.

A 126 mil diameter hole is drilled into endplates of the chamber into which a Teflon tube which fits snugly into the hole and forms the gas seal is inserted. The tube is hollow and allows the wire through the inside and also has a lip so that when the wire comes out it is threaded through a copper tube resting on the lip. The tube is then crimped in two places

with a pneumatic crimper at 80 psi. The wire is threaded through the other side, put through the copper tube, and tensioned.

The tension is applied in a very simple way. A hemostat is attached to the wire and, from this, a weight is suspended. The sense wire is 1.3 mil stableohm tensioned at 65 g. The HV wire is 5 mil stainless steel wire with gold plating tensioned at 60 g. After the tension is set the opposite copper tube is slid into place and crimped.

The value for the tension was chosen by finding the tension at which the wire, broke for the stableohm, or slipped out of the crimp for the hv wire, finding the tension that was needed to keep the wire from being moved by the electrostatic field, and then choosing a tension in the middle of those two. The crimping pressure was chosen in a similar manner. The most important thing was to crimp it as tight as possible to keep the wire from slipping out yet to not make the pressure so great that it pinched off the wire inside the copper tube. Since the crimper is not able to crush the copper tube, we ended up using the maximum rated pressure for the crimper. This is also a function of how the jaws of the crimper are ground and if the crimping area is decreased the operation pressure will also have to be decreased.

## **References**

- [1] D. L. Adams, N. E. Davison, G. Mutchler, P.J. Riley, et al, Research Proposal 1097, LAMPF
- [2] D. L. Adams, N. E. Davison, G. Mutchler, P.J. Riley, et al, Research Proposal 1097 Update, LAMPF
- [3] Particle Data Table
- [4] F. Sauli, Principle of Operation of Multiwire Proportional and Drift Chambers,
- [5] A. Breskin, G. Charpak, F. Sauli, Recent Observations and Measurements with High-Accuracy Drift Chambers, Nuclear Instrumentation Methods 124, 189, (1975)
- [6] J. Groh, E. Schenuit, H. Spitzer, Computer Simulation of Electron Avalanches in Argon-Methane Filled Wire Chambers, DESY 90-023, (March 1990)
- [7] T. J. Killian, Accurate Computer Simulation of a Drift Chamber, Nuclear Instrumentation Methods 176, 355, (1980)
- [8] A. Weltin, Analytic Solution of the Potential and Electric Field of a Jet Type Drift Chamber, Nuclear Instrumentation Methods in Physics Research A264, 213
- [9] G. A. Erskine, Electrostatic Problems in Multiwire Proportional Chambers, Nuclear Instrumentation Methods 105, 565, (1972)
- [10] P. Morse, H. Feshbach, Methods of Theoretical Physics, McGraw-Hill Book Company, NY, (1953)
- [11] M. Abramowitz, I. Stegun, Handbook of Mathematical Functions, Dover Publications, NY, (1970)
- [12] G. Charpak, D. Rahm, H. Steiner, Some Developments in the Operation of Multiwire Proportional Chambers, Nuclear Instrumentation Methods 80, 13, (1970)
- [13] C. Biino, R. Mussa, S. Palestini, N. Pastrone, L. Pesando, A Very Light Proportional Chamber Constructed with Aluminized Mylar Tubes for Drift Time And Charge Division Readouts, IEEE Trans. Nucl. Sci. 36, 98-100,(1989)
- [14] A. Manarin, L. Pregernig, M. Rabany, R. Saban, G. Vismara (CERN), Drift Chamber Electronics with Multihit Capability for Time and Current Division Measurements, Nucl. Instrum. Methods 217, 335-343, (1983)
- [15] D. M. Binnie, Charge Division and Precision Timing in a Drift Chamber, Nucl. Instrum. Methods 192 , 231-233, (1982)
- [16] S. Bartalucci, R. Bertani, S. Bertolucci, M. Cordelli, R. Dini, P. Giromini, M. Pallotta, A. Rutili, A. Sermoneta, M. Spadoni , Test of a Drift Chamber with

- Second Coordinate Readout by Charge Division, Nucl.Instr.Meth., 192, 223, (1982)
- [17] G. C. Barbarino, L. Cerrito, G. Paternoster, S. Patricelli, Measurement of the Second Coordinate in a Drift Chamber Using the Charge Division Method, Nucl. Instr. Meth. 179, 353, (1981)
- [18] L. Baksay, A. Boehm, M. Bozzo, R. Ellis, H. Foeth, R. Hammarstrom, A. Kernan, B. Naroska, A. Staude, P. Strolin, C. Rubbia, A Proportional Chamber with Two-Dimensional Readout Using Drift Time and Current Division, Proceedings, High Energy Instrumentation Conference, Frascati, 256-258, (1973)
- [19] H. Haggerty, H. Janelli, Two-Dimensional Readout of a Drift Chamber Using Current Division, FERMILAB-TM-0718, Mar 22, (1977)